



東京大学
THE UNIVERSITY OF TOKYO

Diploma Thesis

From Nature to Network: Harnessing Caffeic Acid, Monolignols, and Lignosulfonate in Metal-Phenolic Network Assemblies

Submitted at TU Wien, Faculty of Technical Chemistry by

Daniela TOMASETIG

1180860

Under supervision of

Univ.Prof. Dipl.-Ing. Dr.techn. Anton Friedl

Assoc.Prof. Dr. Hirotaka Ejima

Institute of Chemical, Environmental and Bioscience Engineering, E 166

Ich habe zur Kenntnis genommen, dass ich zur Drucklegung meiner Arbeit unter der Bezeichnung

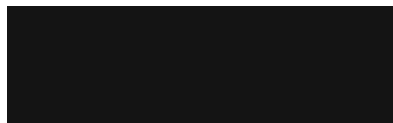
Diploma Thesis

nur mit Bewilligung der Prüfungskommission berechtigt bin.

Statutory Declaration

I hereby declare that I have completed this diploma thesis independently and that no other aids have been used than those I have cited as sources. Literal and analogous quotations have been marked accordingly.

Wien am 31.10.2023



Daniela Tomasetig

Acknowledgements

I want to thank Ejima Hirotaka for accepting me into his research group at Tokyo University in Japan, as well as Anton Friedl for supervising me. Special thanks also go to Chenyu Wang for helping me with my research and for always being willing to listen to my questions and problems.

Thanks to the JASEC (Japan Austria Science Exchange Center) of TU Wien, especially Thomas Rief, for helping me to plan my stay in Japan and for providing me with a Joint Study scholarship. I'm also grateful to Bernhard Lendl for providing me with an additional scholarship and of course to the Austrian State offering financial support through my whole bachelor and master and enabling me to study in the first place.

Last but not least, I want to thank my family and friends for supporting me. Thanks to you, studying at university was a great experience for me.

Abstract

Metal-phenolic networks (MPNs) can be easily formed in a self-assembly process by combining phenol and metal ion solutions. They can be used to coat various materials and potential applications of MPNs include the formation of capsules for drug delivery, reversible coating of microorganisms for protection or proliferation inhibition, metal sequestration or hair dyeing.

In this work, several new phenolic candidates for MPN formation were investigated. Caffeic acid, sodium lignosulfonate and the monolignols coniferyl alcohol, sinapyl alcohol and paracoumaryl alcohol were examined and compared with tannic acid as reference. The formation of MPNs was successful using caffeic acid and lignosulfonate with Fe^{3+} as metal-ion. The new materials were characterized and used to form thin films on various substrates including polystyrene and glass. By dissolving the substrate, free-standing capsules were formed. The thin films could be disassembled by changing the pH of the surrounding solution or adding a chelating agent such as EDTA. Furthermore, the caffeic acid- Fe^{3+} and lignosulfonate- Fe^{3+} MPNs were used to dye human hair in emerald-green or straw-yellow color respectively.

Kurzfassung

Metall-Phenolische Netzwerke (MPNs) können einfach in einem Selbstanlagerungsprozess gebildet werden, indem Phenol- und Metallionenlösungen kombiniert werden. Sie können benutzt werden, um verschiedenste Materialien zu beschichten und potenzielle Anwendungen von MPNs beinhalten die Erzeugung von Kapseln zum Wirkstofftransport, reversible Beschichtungen von Mikroorganismen, um diese zu schützen oder ihre Teilung zu stoppen, Metall Sequestrierung oder Haare färben.

In dieser Arbeit wurden mehrere neue phenolischen Kandidaten für die Bildung von MPN untersucht. Kaffeesäure, Natrium-Ligninsulfonat und die Monolignole Coniferylalkohol, Sinapylalkohol und p-Cumarylalkohol wurden untersucht und mit Tanninsäure als Referenz verglichen. Die Bildung von MPNs war mit der Verwendung von Kaffeesäure und Ligninsulfonat mit Fe^{3+} als Metallion erfolgreich. Die neuen Materialien wurden charakterisiert und sie wurden benutzt, um dünne Filme zu bilden und damit verschiedenste Substrate, wie Polystyrol und Glas, zu beschichten. Durch Auflösen des Substrates wurden frei-stehende Kapseln geformt. Die dünnen Filme konnten aufgelöst werden, indem der pH-Wert der umgebenden Lösung verändert wurde, oder indem Chelatbildner, wie EDTA, zugegeben wurden. Außerdem wurden die Kaffeesäure- Fe^{3+} und Ligninsulfonat- Fe^{3+} MPNs verwendet, um menschliches Haar smaragdgrün und strohgelb zu färben.

Table of contents

Acknowledgements	I
Abstract	II
Kurzfassung.....	III
Table of contents	IV
1 Introduction	1
1.1 Lignin and its derivatives	1
1.2 Metal Phenolic Networks	4
1.3 Analytical Methods.....	5
2 Experimental Part.....	10
2.1 Materials	10
2.2 Instruments	11
2.3 QCM-Experiments.....	12
2.4 UV-Vis Experiments	14
2.5 Preparation of MPN-capsules	17
2.6 Contact Angle Measurement	18
2.7 Hair dyeing experiments.....	19
2.8 FTIR Measurements	20
3 Results and Discussion.....	21
3.1 QCM Experiments	21
3.2 UV-Vis experiments	26
3.3 MPN Capsules	36
3.4 Contact angle	41
3.5 Hair dyeing	43
3.6 FTIR-spectra.....	44
4 Summary	50
Daniela Tomasetig	IV

Table of contents

5	Conclusion.....	54
6	Outlook.....	55
	List of Abbreviations.....	56
7	References	57
8	List of Figures	62
9	List of Tables.....	66
10	Appendix	68

1 Introduction

Metal phenolic networks (MPNs) have potential for many different uses, as they can be used for cell encapsulation, for metal sequestration or as hair dye [1–3]. Coordinative bonds can be formed between electron donating phenols and transition or main group metals with vacant orbitals [4]. MPNs can be assembled easily using aqueous solutions under mild conditions. One step assembly, as well as multistep and spray assembly for the MPNs formation have been reported. All of these assembly methods have in common that aqueous solutions can be used and no heating or cooling is needed, which makes the assembly processes environmentally friendly [5,6]. To expand the toolbox of usable phenols and to investigate the limits of MPN formation compounds derived from lignin such as caffeic acid, monolignols or lignosulfonate shall be examined for MPN assembly in this thesis. To verify the success of the formation of MPNs different analytical methods and devices such as quartz crystal microbalance (QCM), Ultraviolet-visible (UV-Vis) and Fourier-transform infrared (FTIR) spectroscopy, optical microscopy, electron microscopy and atomic-force-microscopy (AFM) were used.

1.1 Lignin and its derivatives

Lignin is one of the most abundant macromolecules on earth [7]. Besides cellulose it is the main building material of woody biomass and the reason for the pressure resistance of plant cell walls. It also plays an important role in protecting plants from biodegradation by microorganisms because only a few organisms can degrade it [8].

There are three main phenolic building blocks of lignin often referred to as monolignols. The monolignols are paracoumaryl alcohol (pCA), coniferyl alcohol (CA) and sinapyl alcohol (SA)(see Figure 1) [8]. All of them have an unsaturated propyl sidechain containing one hydroxyl group, as well as one hydroxyl group at the benzene ring, but no vicinal diol group. Coniferyl alcohol and sinapyl alcohol additionally have methoxy groups bonded to the benzene ring. The monolignols were examined as possible phenols for MPN assembly.

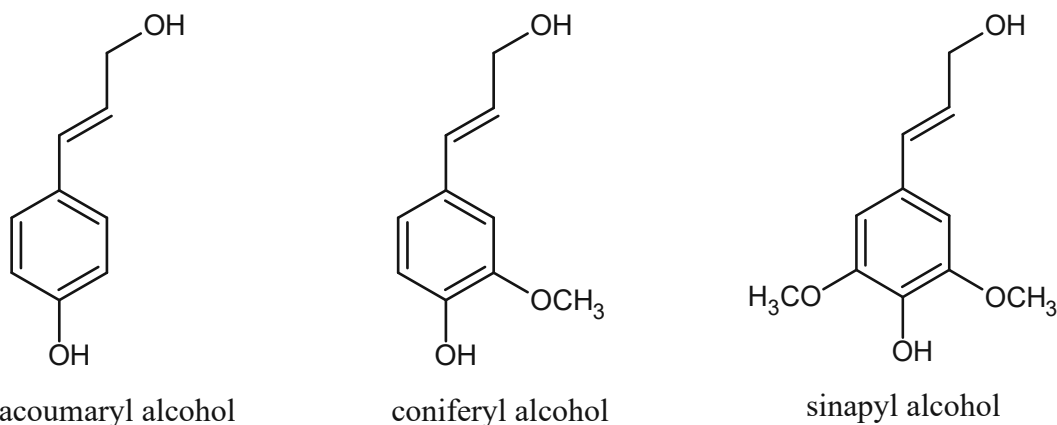


Figure 1: Chemical structure of the 3 main monolignols paracoumaryl alcohol, coniferyl alcohol and sinapyl alcohol

Caffeic acid (CaAc), which was also examined in this thesis, is a precursor in the biosynthesis of sinapyl and coniferyl alcohol. It is formed after various steps in the phenylpropanoid pathway usually starting with phenylalanine as initial substrate. In contrast to the monolignols it contains a vicinal diol group which generally favors the formation of MPNs [8,9]. The structure of caffeic acid can be seen in Figure 2. Caffeic acid can be found in many plants, such as coffee, thyme or sage [10].

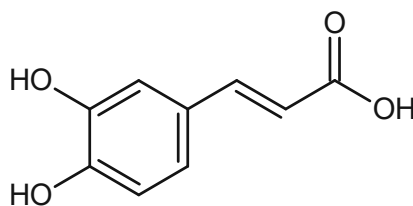


Figure 2: Chemical structure of caffeic acid

The monolignols are polymerized to lignin in a radical reaction and build a meshed irregular network. To catalyze the polymerization reaction of the monolignols outside of the cells in the apoplast plants use lignin peroxidase as catalyst which forms radicals (most likely H₂O₂). Natural lignin in plants has no uniform structure. The ratio of the monolignols in lignin varies, as well as the bonding types. This makes the study of the behavior of lignin difficult because each lignin behaves slightly different [11]. Due to its poor solubility in water and because lignin was already successfully examined for MPN formation, it wasn't investigated in this thesis [12].

Wood contains about 20-30 % lignin. In pulp and paper processes this lignin is removed from the wood, making it an abundant by-product. One of the processes to remove the lignin is called sulfite process. In this process different sulfites are used to hydrolyze the ether bonds in lignin and build phenolates. This phenolates then get sulfonated, which turns them water soluble as illustrated in Figure 3 [13].

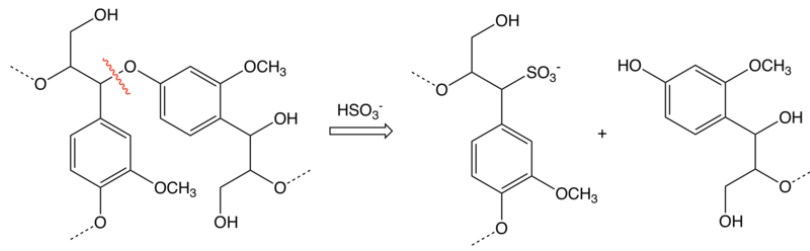


Figure 3: Idealized scheme of sulfonation and hydrolyzation of lignin during sulfite process (Source: Wikimedia)

The resulting sulfur content of liginosulfonate is usually higher than 5 % [14]. Liginosulfonate is known to form complexes with Fe^{3+} involving hydroxy, phenol hydroxyl, carboxyl and sulfonate groups for bonding [15]. The liginosulfonate used in this thesis was, obtained from needle-leaved and broad-leaved trees by using sodium sulfite as digestive reagent [16]. The possible structure of liginosulfonate is illustrated in Figure 16.

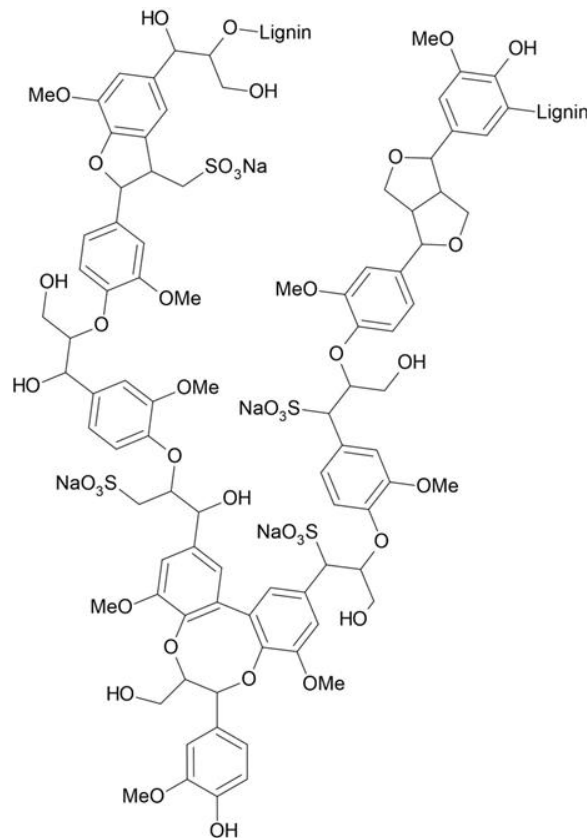


Figure 4: "Generic" structure of liginosulfonates. Adapted from [17].

1.2 Metal Phenolic Networks

Metal phenolic networks are formed through diverse metal-organic interactions such as cation-, π -, coordination-, redox- and dynamic covalent interactions. There are various examples of metal-phenolic interactions in nature and human history. Mussel byssus exhibits high stiffness and extensibility, which can be attributed to Fe^{3+} - catechol complexes. Gall ink, which contains tannins and Fe^{2+} ions was already used in the Middle Ages in Europe [3,18]. The versatility of MPNs extends to the selection of metals for their formation, alongside the vast array of potential phenols. More than 8000 polyphenols have been identified as of today [19]. In this thesis, Fe^{3+} ions are mainly used to form metal phenolic networks.

It is hypothesized that coordination interactions are the predominant force in the assembly process for transition metal ions. Notably, the pH value can, as a critical factor, influence MPN formation, dictating the nature of the complex formed, as illustrated in Figure 5.

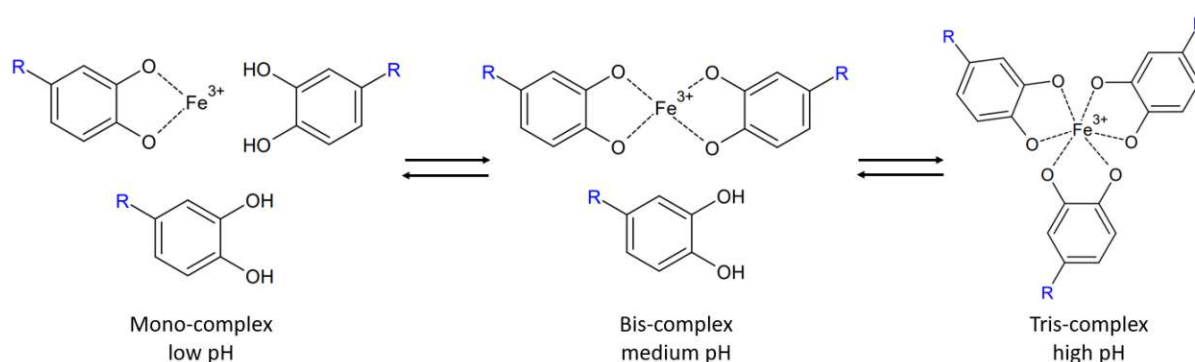


Figure 5: Formation of mono-, bis- and tris-complexes between Fe(III) and Phenols at different pH values.

Parameters such as binding strength, stability and binding site availability are important for film formation. Studies suggest that vicinal diol groups at the benzene ring might be necessary for the formation of MPNs [20]. Tannic acid (TA) is one of the commonly used phenolics for the formation of MPNs. It has five galloyl moieties and a glucose unit as core, making it possible to bind multiple metal ions. It forms intensely colored complexes with ferric ions (Fe^{3+}). The ideal structure of tannic acid can be seen in Figure 6, but commercially available tannic acid is not pure, as some other polygalloyl glucose units are present. Tannic acid is a suitable reference for the different experiments performed [21,22].

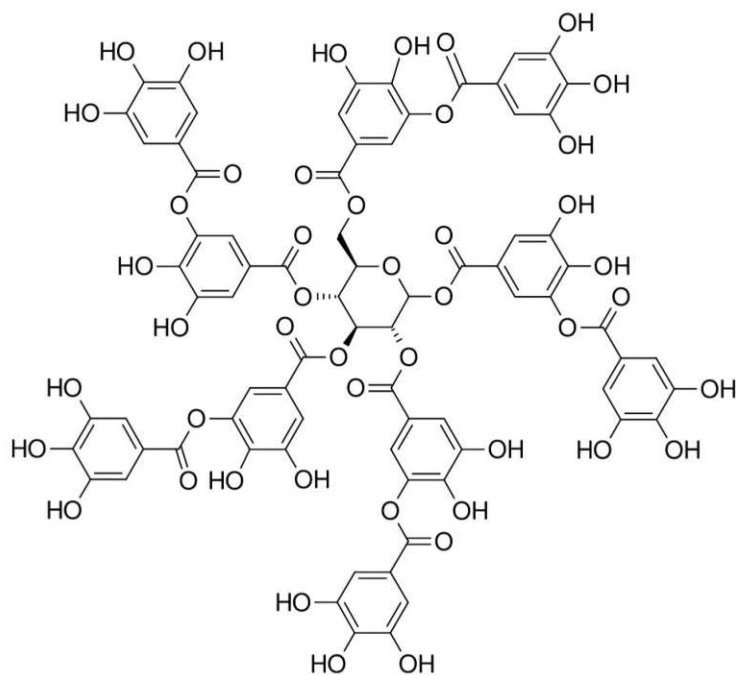


Figure 6: Chemical structure of tannic acid

MPNs assemble spontaneously and rapidly without the need for supplementary heating. Reported processes include simple mixing of the phenolic and metal ion solution with possible subsequent pH adjustment or consecutive dipping of the template into the metal ion and phenolic solution as well as spraying the template with the metal ion and phenolic solution consecutively. Typically MPN films are approximately 5 to 50 nm thick [5,6,20,23]. However macroscopic film assembly methods with film thickness in micrometer range have been reported as well [24].

1.3 Analytical Methods

Quartz Crystal Microbalance

Quartz Crystal Microbalances (QCM) can be used to detect small mass differences down to 1 ng, which makes it possible to detect the formation of thin and therefore lightweight MPN-films. The change of the vibration frequency of a quartz crystal is dependent on the mass of the layer attached to the crystal and can be determined by putting it in an oscillator circuit as frequency determining part. To make this possible a conductive layer needs to be evaporated on the crystal, most commonly gold. Only the middle part of the crystal takes part in the vibration, which makes it possible to attach the border of the crystal to electrodes for measurement without influencing them measured value. Some limiting factors for the precision of the balance are temperature changes and changes in air humidity, which will influence the

vibration frequency of the crystal. The uniformity of the layer that shall be measured is of importance because the sensitivity of the crystal is the highest at the center and decreases towards the borders. To calculate the mass difference of the QCM-chip the Sauerbrey equation (Equation 1) is commonly used [25].

$$\Delta F = -\frac{2F_0^2}{A\sqrt{\mu_q\rho_q}}\Delta m \quad \text{Eq. 1}$$

ΔF ... frequency change of the quartz crystal [s^{-1}]

Δm ... mass difference [kg]

F_0 ... natural frequency of the quartz crystal [s^{-1}]

A ... area of the quartz crystal [m^2]

ρ_q ... density of the quartz crystal [$kg\ m^{-3}$]

μ_q ... Shear modulus of the quartz crystal [$kg\ m^{-1}\ s^{-2}$]

UV-Vis Spectroscopy

UV-Vis Spectroscopy can be used to examine the absorption of light by compounds in a wavelength range from 200 – 800 nm. This can be used to obtain structural information about the observed sample and indicate the thickness of the MPN layer. One important empirical law used in UV-Vis spectroscopy (but also other types of spectroscopy such as IR-spectroscopy) is Lambert-Beer (Equation 2) which sets the absorption into direct proportion with the optical path length measured and the concentration of the absorbing compound. Because this is an empirical law, it does not always apply exactly, especially at low and high absorptions deviations are possible. Absorption bands in the UV-Vis region are typically broad. Water's lack of absorbance in the UV-Vis spectral region facilitates feasible measurements within aqueous solutions [26,27].

$$A = \log\left(\frac{I_0}{I}\right) = \varepsilon(\lambda) * c * l \quad \text{Eq. 2}$$

A ... absorbance

$\varepsilon(\lambda)$... decadic extinction coefficient of the compound [$l\ mol^{-1}\ cm^{-1}$]

c ... concentration of the compound [mol/l]

l ... optical path length [cm]

FTIR Spectroscopy

FTIR spectrometers are mostly used in the mid-IR range from 400 to 4000 cm^{-1} (equaling a wavelength of 2500 to 25 000 nm) to measure the absorption of light by the sample in that range caused by molecular vibrations. The bands are sharp compared to UV-Vis spectroscopy, but water absorbs strongly in the IR-region making measurements in aqueous solution difficult. The bands seen in IR-spectra can be used to identify substances and vibrations of specific functional groups can be assigned to the bands. The measurements are often, like in this thesis, conducted using the attenuated total reflection (ATR) method. With this method, the light beam is sent towards the sample through an ATR-crystal. On the interface between the sample and the crystal total reflection takes place and an evanescent wave is formed that interacts with the sample. The ATR method requires minimal sample preparation and offers high sensitivity. The penetration depth of this wave is dependent on different factors such as the wavelength of the light and the refraction index of the crystal and the sample. Hence the Lambert-Beer law cannot be applied as easily for calculating concentrations because the optical path length is unknown. [28]

Optical microscopy

Microscopy is used to make small objects visible, that cannot be seen using the naked eye. For this thesis an inverted transmission microscope was used. In transmission microscopy the light passes through the sample that shall be examined. A condenser is used to focus the light on the sample, the light then passes through the objective lenses and the oculars to magnify the image of the sample [29]. The maximum magnification of optical microscopes is limited by the wavelength of the light used to observe the sample. To describe the minimum resolvable separation Abbe's theoretical relationship (Eq. 3), which is deduced from the Rayleigh criterion, can be used [30]. Hence, to further resolve small features of the prepared MPN capsules different analytical methods had to be used.

$$d = 0.61 \frac{\lambda}{n \cdot \sin(\alpha)} = 0.61 \frac{\lambda}{NA} \quad \text{Eq. 3}$$

d ... minimum resolvable separation [nm]

λ ... wavelength of illuminating light [nm]

n ... refractive index between object and objective lens

α ... half-angle subtended by the objective at the object

Electron microscopy

In contrast to optical microscopy, electron microscopy uses electrons instead of light to illuminate the sample. The electrons accelerated towards the sample possess much smaller wavelengths than visible light and therefore smaller distances can be resolved according to Eq 3. The requirement of conducting the process under vacuum conditions is essential to facilitate electron acceleration and unhindered traversal of electrons to the specimen, preventing any preliminary collisions. To focus the electron beam, magnetic lenses are commonly used. Two different types of electron microscopy were used to observe MPN capsules, transmission electron microscopy (TEM) and scanning electron microscopy (SEM).

The principle of TEM resembles the principle of optical transmission microscopy, but instead of a light beam, an electron beam passes through the sample. A multitude of magnification lenses are used, to reach magnifications up to x500 000.

In SEM, a fine beam of electrons is focused on the surface of the sample. The electron beam is used to scan across the sample in a raster or a pattern of parallel lines to receive a 2D picture. Due to the impact of the electrons on the surface different phenomena occur. Secondary electrons, backscattered electrons and radiation are produced and can be detected using different detectors. Secondary electrons are formed after collision of primary electrons from the electron beam with the specimen and provide high-resolution information as well as some information about the topography of the specimen. Backscattered electrons are re-emerged primary electrons after interaction with the sample and help to provide information about the atomic number of the atoms in the specimen. When the electron beam hits the sample electrons from inner shells can be emitted. Subsequently electrons from higher energy shells replace them, emitting radiation providing information about the element involved. This information can be displayed in an energy-dispersive X-ray spectroscopy (EDS) spectrum. [30]

Atomic Force Microscopy (AFM)

Atomic Force Microscopy (AFM) offers the capability to surpass the diffraction limit of optical microscopy, enabling resolutions down to atomic scale. This technique facilitates the imaging of sample shapes at the nanometer level. In AFM a cantilever with a sharp tip at the end, often referred to as probe, is used to scan the surface of a sample. It is possible to scan the surface in two ways. Either the cantilever with the tip moves over the sample or the sample is moved

below the cantilever. The height change of the cantilever caused by the sample can be detected by focusing a laser on the cantilever and detecting the position of the reflected laser. [31]

Intermittent contact mode is a dynamic mode of AFM measurement. The cantilever oscillates at its resonance frequency near the sample surface. This minimizes contact with the sample and results in higher resolution [32].

2 Experimental Part

2.1 Materials

The following phenolic compounds were examined as possible ligands for forming MPNs. Tannic acid was used as reference for MPN formation. Because the water solubility of caffeic acid is very low (~ 1 g/l) it was dissolved in 50 (w/w)% ethanol [33].

- Tannic acid (TA, Sigma Aldrich)
- Caffeic acid (CaAc, Fujifilm Wako Pure Chemicals)
- Para-Coumaryl alcohol (pCA, Toronto Research Chemicals)
- Coniferyl alcohol (CA, Fujifilm Wako Pure Chemicals)
- Sinapyl alcohol (SA, Cayman Chemical)
- Lignosulfonate (LS, Tokyo Chemical Industry co.)

TA and LS were both easy to dissolve in water. pCA was difficult to dissolve in water and 1 g/l didn't dissolve overnight. Sonicating the solution for 30 minutes was necessary to dissolve pCA. CA was similarly difficult to dissolve in water as pCA. Sonicating was necessary to dissolve 1 g/l CA. CA exhibited a vanillin-like odor. SA (1 g/l) was easier to dissolve in water and could be dissolved without sonicating and the solution had a slightly yellow color. 10 g/l of CaAc could not be dissolved in water, since the solubility of CaAc in water is low. Instead, 5 g/l of CaAc were dissolved in a 50 % ethanol/water mixture. Besides the phenolic compounds various other chemicals and materials were used to form MPNs and to conduct the following experiments. MilliQ water with a resistivity greater than $18 \text{ M}\Omega$ was obtained by a Type 1 Merck Ultrapure Water System. MilliQ water was used for all experiments and therefore in the experimental part it is always referred to as water.

- $\text{FeCl}_3 \cdot 6\text{H}_2\text{O}$ (Fujifilm Wako Pure Chemicals)
- $\text{AlCl}_3 \cdot 6\text{H}_2\text{O}$ (Fujifilm Wako Pure Chemicals)
- $\text{ZrCl}_2\text{O} \cdot 8\text{H}_2\text{O}$ (Fujifilm Wako Pure Chemicals)
- $\text{CuSO}_4 \cdot 5\text{H}_2\text{O}$ (Fujifilm Wako Pure Chemicals)
- $\text{MnCl}_2 \cdot 4\text{H}_2\text{O}$ (Fujifilm Wako Pure Chemicals)
- $\text{CoCl}_2 \cdot 6\text{H}_2\text{O}$ (Fujifilm Wako Pure Chemicals)
- 3-(N-morpholino)propanesulfonic acid buffer (MOPS, Dojindo)
- Ethanol, super dehydrated (99.5 %, Fujifilm Wako Pure Chemicals)

- Diethylether (Fujifilm Wako Pure Chemicals)
- Tetrahydrofuran (THF, Fujifilm Wako Pure Chemicals)
- PS-microspheres in aqueous solution, 2.7 %, $\text{\O} = 3 \mu\text{m}$ (Polysciences Inc.)
- Piranha solution (conc. HCl and 30 % H_2O_2 mixture, ratio 3:1)
- NaOH 1 mol/l (Fujifilm Wako Pure Chemicals)
- Concentrated HCl (Fujifilm Wako Pure Chemicals)
- Disodium dihydrogen ethylenediaminetetraacetic acid, (EDTA, Tokyo Chemical Industry co.)
- (+) Sodium L-ascorbate (Fujifilm Wako Pure Chemicals)

2.2 Instruments

QCM-measurements were performed with a Quartz Crystal Microbalance QCM922A (Seiko Instruments). For this measurement rectangular gold QCM crystals as depicted in Figure 7 were used (QA-A9M). The diameter of the round measurement circle was 5 mm. The viability of the crystal was controlled during each measurement by checking the resistance. High resistance values indicated insufficient contact between the electrode of the crystal and the sample holder and would result in faulty frequency measurements. For each measurement the resistance was below 50 Ω .

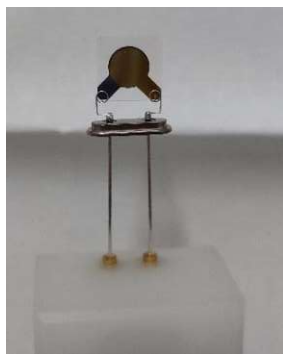


Figure 7: QCM crystal inserted in sample holder.

FTIR measurements were performed using an IRSpirit-T FTIR-Spectrometer by Shimadzu. The spectrometer was equipped with a diamond ATR-Element (GladiATR).

UV-Vis spectra were taken using a NanoDrop One C UV-Vis Spectrometer (Thermo Scientific) with single use cuvettes made of Poly(methyl methacrylate) (PMMA). The measurement range of the spectrometer was between 190 and 850 nm with datapoints every 0.5 nm. PMMA cuvettes can only be used at wavelengths greater than 275 nm therefore the effective measurement range was 275 nm to 850 nm.

The pH-values of the solutions were measured using a small handheld LAQUAtwin pH-meter (Horiba). The pH-meter was calibrated regularly by using pH 4.01 and pH 6.86 calibration solutions.

Optical Microscopy pictures were taken with a Nikon Eclipse TE2000-U inverted microscope.

Scanning electron microscopy pictures were taken using an JEOL JCM-7000 SEM. To prepare the samples a platin sputter coater (Jeol JEC – 3000 FC) was used. For coating a current of 30 mA and a coating time of 15 to 60 s were chosen.

Transmission electron microscopy pictures were taken using a JEOL JEM-1400 electron microscope. The used copper grid for the observation was priorly hydrophilized using a Jeol HDT-400 hydrophilic treatment device (utilizing plasma).

AFM images were obtained using a NanoWizard AFM intermittent contact mode.

For contact angle measurement a contact angle goniometer was used, and the images were analyzed using a contact angle measurement plugin for ImageJ.

2.3 QCM-Experiments

The MPNs synthesized for this thesis were prepared in two different ways. The first way, described in chapter 2.3.1 basically consists of mixing the components for MPN formation stepwise together. In the second way described in chapter 2.3.2 the substrate (= QCM crystal) is consecutively dipped into phenolic and Fe^{3+} solution.

2.3.1 Multistep preparation of MPNs by mixing solutions

The QCM-crystals were cleaned before usage by soaking them in piranha-solution (conc. H_2SO_4 and 30 % H_2O_2 mixed 3:1) for an hour. Subsequently, they were rinsed with water, air dried using a stream of N_2 and weighed. Afterwards the crystal was put into a glass vial and 500 μl of water and 5 μl of phenolic solution (concentration, see Table 1) were added. The mixture was homogenized thoroughly using a vortexer and 5 μl Fe^{3+} solution (37 mmol/l) were added. The mixture was immediately homogenized. To stabilize the MPNs 500 μl of MOPS buffer (10 mmol/l) with a pH of 7.4 was added and the mixture was homogenized once more. The vial was then flushed with water and the QCM crystal was taken out of the vial, rinsed with water, air dried using a stream of N_2 and weighed. This cycle was then repeated 20 times to observe the mass gain of the QCM crystal. To determine the blind mass-gain, this experiment was additionally carried out in two different blind versions. In one version no

phenolic solution was added. For the other version no phenolic solution and no MOPS buffer were added.

Table 1: Parameters for the coating process with MPNs of the QCM crystal stating the amount and concentration of the phenol and iron solution added and the number of repetitions for each experiment. For the coating process the phenol and iron solution are combined with water and MOPS is added subsequently.

	c_{Phenol} (mmol/l)	V_{Phenol} (μl)	$c_{\text{Fe}^{3+}}$ (mmol/l)	$V_{\text{Fe}^{3+}}$ (μl)	V_{MOPS} (μl)	repetitions
TA	24	5.0	37	5.0	500	3
pCA	19	5.0	37	5.0	500	3
blind (no phenol)	0	0	37	5.0	500	1
blind (only Fe added)	0	0	37	5.0	0	1

2.3.2 Multistep preparation of MPNs by dipping

This experiment was based on studies carried out by Rahim et. Al [23]. The clean QCM crystals were dipped into the phenolic compound solution and the Fe^{3+} solution consecutively. The concentration of the phenolic compound solutions was 1 g/l, and the phenolic compounds were dissolved in MOPS buffer solution (10 mmol/l) with a pH of 7.4 instead of water. The MOPS solution should stabilize the formed MPN network. An aqueous Fe^{3+} solution (3.7 mmol/l) was prepared freshly every day by dissolving $\text{FeCl}_3 \cdot 6\text{H}_2\text{O}$ in water. Before usage the QCM-crystals were cleaned using piranha-solution (conc. H_2SO_4 and 30 % H_2O_2 mixed 3:1), rinsed with water and air dried using a stream of N_2 . The cleaned chip was weighed, dipped into phenolic solution for 10 min, rinsed with water, dried using a stream of N_2 and weighed again. The dipping, rinsing, drying, and weighing process was then repeated using the Fe^{3+} -solution. This cycle was repeated 15 times (excluding the cleaning process with piranha solution at the beginning) to add more layers to the crystal. A blank test was carried out by replacing the phenol containing MOPS solution with no phenol containing MOPS solution for comparison. The concentration of the phenol solution for each experiment is noted in Table 2.

Table 2: Concentrations of the Phenol-solutions used for the MPN dipping experiment of the QCM crystal and number how often each experiment was repeated. The QCM crystal is dipped into the solutions in succession to coat it.

Phenol	c_{Phenol} (g/l)	c_{Phenol} (mmol/l)	repetitions
TA	1	0.588	3
pCA	1	6.66	3
CA	1	5.55	3
SA	1	4.76	1
LS	1	-	3
blind	0	0	3

2.3.3 Disassembly experiments

For the disassembly experiments either coated QCM-crystals from the multistep preparation by dipping (chapter 2.3.2) were used or the dipping process was imitated using shorter dipping times and skipping most weighing processes in between. The crystals were coated till they had gained roughly 1000 ng of mass. The crystals were then weighed and put into a glass vial with either a pH adjusted solution (pH 2, 3 and 5) or into an EDTA solution (10 mmol/l, pH - 4.8). The pH of the solutions was adjusted using HCl, no additional buffering substances were added to prevent unwanted interactions. The pH of the solutions was checked occasionally and readjusted if necessary. After set time periods the chips were removed from the solution, rinsed with water, air dried using a N₂-stream, weighed, and put back into the solutions. This experiment was only carried out using LS-Fe and pCA-Fe coatings as summed up in Table 3.

Table 3: Summary of QCM disassembly experiments carried out. Including the mass of the MPN layer prior to disassembly, the disassembly conditions, and the type of MPN coating.

	condition	initial mass [ng]
pCA-Fe	pH 2	1099
pCA-Fe	pH 3	1026
pCA-Fe	pH 5	1299
pCA-Fe	EDTA	1123
LS-Fe	pH 2	729
LS-Fe	pH 5	881
LS-Fe	EDTA	1448

The QCM results proved to be unstable and had a poor reproducibility, consequently they were replaced with UV-Vis measurements.

2.4 UV-Vis Experiments

A multitude of experiments using UV-Vis spectroscopy were performed. UV-Vis Spectra of the pure components and complexes formed after combining metal- and phenol-solutions were obtained to gain information about the interaction between the metal and phenol. The optimal ratio of phenol to iron was determined by mixing them in different ratios and measuring spectra. For the CaAc-Fe complex, the dependence of the pH on the color of the complex and MPN-layer formation was examined. Different metal-ions (e.g., Mn²⁺, Al³⁺, Cu²⁺, Co²⁺ and Zr⁴⁺) were tested as possible candidates for MPN formation. The time-dependence of MPN film formation as well as the growth of multilayer MPN-films was monitored by coating cuvettes. MPN coated cuvettes were filled with different disassembly solutions and the disassembly was monitored

using UV-Vis spectroscopy to gain information about the stability of the MPN films. Water served as the background for all UV-Vis measurements. Single use PMMA cuvettes with an optical path length of 1 cm were used.

2.4.1 Complex characterization and Phenol:Fe³⁺ ratio optimization

The raw phenolic solutions and Fe³⁺ solutions were measured as well as mixtures of phenolic and Fe³⁺ solutions to visualize the ligand-to-metal charge transfer (LMCT) bands. The optimal ratio of phenolic compound to Fe³⁺ was determined by mixing the phenol and Fe³⁺ solution in different ratios, keeping the total volume of phenol and Fe³⁺ solution used constant and measuring the absorption as well as taking pictures and observing precipitation behavior. The ratio optimization experiment parameters are summed up in Table 4. Note that the mass ratio for LS-Fe was calculated using the mass of LS and the mass of FeCl₃·6H₂O used.

Table 4: Concentrations and volumes of the Phenol and Fe³⁺ solutions mixed to optimize the ratio. Additional water was added for CaAc-Fe to decrease the intensity of the complex. CaAc-Fe and pCA-Fe were mixed to achieve specific molar ratios. For LS-Fe mass ratios (mass LS:mass FeCl₃·6H₂O) were used, since the molar mass of LS is unknown.*concentration of FeCl₃·6H₂O

	C _{Phenol}	C _{Fe-salt}	V _{Phe} +V _{Fe}	V _{H₂O}	Phe:Fe ratios examined
CaAc - Fe	27.8 mmol/l	37 mmol/l	100 µl	900 µl	4:1, 2:1, 1:1, 1:2, 1:4
LS - Fe	1 g/l	1 g/l *	1000 µl	-	4:1, 2:1, 1:1, 1:2, 1:4
pCA - Fe	14.8 mmol/l	14.8 mmol/l	1000 µl	-	32:1, 16:1, 4:1, 3:1, 2:1, 1:1, 1:2, 1:3, 1:4, 1:16, 1:32

2.4.2 Determination of pH influence on CaAc-Fe complex

For the CaAc and Fe³⁺-complex the pH was adjusted to visualize the impact of pH change on complex formation. Water (2 ml), CaAc (25 µl, 27.8 mmol/l) and FeCl₃·6H₂O solution (37.5 µl, 37.0 mmol/l) were mixed in cuvettes. Afterwards, the pH of the mixtures was adjusted using conc. HCl and NaOH solution (1 mol/l). The pH value of the mixtures was incrementally adjusted from 1 to 11 with a step size of 1. Following several days of allowing the solution to sit, the cuvettes were rinsed with water multiple times, subsequently filled with water, and spectra of the MPN coated cuvettes were measured. This process aimed to ascertain the pH at which MPN layers were formed.

2.4.3 Examination of different metal ions for MPN formation

Metal-ions were tested for their ability to form MPNs. Solutions of AlCl₃·6H₂O, ZrCl₂O·8H₂O, CuSO₄·5H₂O, MnCl₂·4H₂O and CoCl₂·6H₂O with a concentration of 27.8 mmol/l were prepared. The metal solutions were mixed with phenolic solutions (CaAc solution, c_{CaAc} = 27.8 mmol/l and LS-solution, c_{LS} = 10 g/l). The behavior upon mixture (color change

or precipitation) was then used to estimate whether those metals are promising candidates for MPN formation or not.

2.4.4 Preparation of multilayer MPN-films in cuvettes

PMMA cuvettes were coated with MPN layers and UV-Vis measurements were conducted. To coat the cuvettes a predetermined amount of water, phenolic compound solution and Fe^{3+} solution (see Table 5) was pipetted into the cuvette and the solution was homogenized using a vortexer. To add additional layers, the solution was removed, and the coating procedure was repeated. The cuvettes were coated with 30 layers and the UV-Vis absorption of the layer formed on the cuvette walls was observed after every 5th layer. Before each UV-Vis measurement the cuvettes were rinsed and filled with water. A clean cuvette filled with water was used as blank. The amount of phenolic solution and Fe^{3+} solution was varied to gain information on the concentration dependence of the layer build-up (Table 5).

Table 5: Concentration of Phenol and Metal-salt used for the stepwise coating of the UV-Vis cuvettes. Water, phenol- and iron-solution were mixed to reach the concentrations stated and to coat the cuvettes.

Coating	c_{Phenol} (g/l) (after mixing)	$c_{\text{metal-salt}}$ (g/l) (after mixing)	repetitions
TA - Fe	0.24	0.06	3
TA - Fe	0.48	0.12	6
TA - Fe	0.96	0.24	3
TA - Fe	4.00	1.00	1
CaAc - Fe	0.24	0.71	3
CaAc - Fe	0.48	1.43	3
CaAc - Fe	0.95	2.86	3
CaAc - Zr	0.25	0.45	1
LS - Fe	0.50	0.50	4
LS - Fe	1.00	1.00	4
LS - Fe	2.00	2.00	4
LS - Zr	0.50	0.45	1
pCA - Fe	0.29	0.53	1

2.4.5 Examination of time dependence of MPN-film formation

A preset amount of water, Fe^{3+} solution and phenolic compound solution was put into the cuvette. Before measurements the solution was removed from the cuvette and stored in another vial and the cuvette was rinsed and filled with water. After the measurement the water was removed, and the coating solution was returned to the cuvette to measure the time dependence of the assembly process.

Table 6: Concentration of Phenol and Metal-salt used for the examination of time on the coating of the UV-Vis cuvettes. The coating solution containing the phenol and metal were kept in the cuvette and only removed for the measurement.

	c_{Phenol} (g/l) (after mixing)	c_{Metal-salt} (g/l) (after mixing)	repetitions
TA - Fe	0.48	0.12	3
CaAc - Fe	0.48	1.43	4
LS - Fe	1.00	1.00	3

2.4.6 Disassembly experiments

Precoated cuvettes were used for this experiment. To examine the disassembly behavior solutions at different pH (1, 4, 7.4, 12) were prepared as well as EDTA (10 mmol/l, pH - 4.8) and sodium ascorbate (10 mmol/l, pH = 7.3) solution. To adjust the pH of the acidic and basic solutions HCl and NaOH were used. The cuvettes were filled with the prepared solution. Before the measurement the solution was removed, the cuvette was rinsed with water and filled with fresh disassembly solution. This approach helped prevent the undesirable impact of dissolved MPN components on the UV-Vis spectra. At the beginning measurements were conducted more frequently, because it was expected that the film formation would be faster at first and slow down later. These experiments were carried out to examine the kinetics for TA-Fe, CaAc-Fe and LS-Fe disassembly.

2.5 Preparation of MPN-capsules

To prepare MPN-capsules different approaches were examined. The standard procedure is as follows. 185 μl of the PS-particle solution (2.7 %) and 305 μl of water were mixed in a vial. The phenolic solution was added, and the mixture was homogenized using a vortexer. Subsequently the Fe^{3+} solution was added, and the mixture was homogenized immediately. 500 μl of MOPS-buffer (10 mmol/l) were added. After homogenization the mixture was centrifuged (6200 rpm, 200 G) till the particles settled, the supernatant solution was removed, water was added, and the mixture was homogenized. This washing step was repeated one time if more layers should be added to the particles or two times if the PS-particles were to be dissolved afterwards. If more layers were added, the above-described coating process was repeated, but water was added instead of PS-microsphere solution, to ensure a constant concentration of coating solution (before centrifugation the overall volume of the mixture should always be approximately 1 ml). After finishing the coating and washing 2 to 3 times with water, the mixture was washed another 2 to 3 times with THF to dissolve and remove the

PS. The remaining capsules were dissolved in water again. The sequence of steps for the preparation of MPN-capsules is summed up in Figure 8.

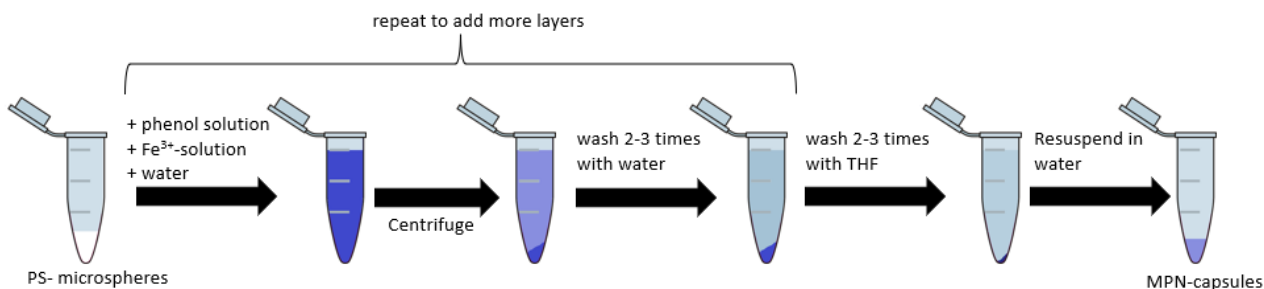


Figure 8: Illustration of the capsule formation process. The phenol- and Fe³⁺ solution are added to the vial with the microspheres. Washing takes place by centrifuging and replacing the supernatant solution with water. To dissolve the PS, the MPN-capsules are washed with THF 2 or 3 times, and the capsules are resuspended in water.

To check if the process was successful, 1-2 μl of the capsule-solution was put on a glass slide and examined with an optical microscope. The capsules were further examined using SEM TEM and AFM. For SEM measurements 1 μl of the capsule-solution was dropped on a Piranha washed silicon substrate and the water was evaporated completely. Afterwards the sample was coated with a platin sputter coater to increase conductivity. For TEM observation, 2 μl of the capsule solution was dropped onto a plasma treated copper grids. After 2 min, the excess liquid was carefully removed using filter paper. For AFM measurements a glass slide was pre-cleaned in Piranha solution for 30 min, rinsed with MilliQ water and air dried. 1 μl of the capsule solution was dropped on the cleaned glass slide and it was waited till the water completely evaporated.

2.6 Contact Angle Measurement

For contact angle measurements, glass slides (Matsunami micro cover glass) were coated with MPN layers. The glass slides were either used directly without prior washing or prewashed using the following procedure. The glass slides were prewashed by putting them into water and sonicating them for 20 min. They were subsequently put into ethanol and sonicated for another 20 minutes. Before coating the glass slides were rinsed with water and air dried [34]. For coating the glass slides were put into glass vials and the phenol and Fe³⁺ solution was added (Figure 9).

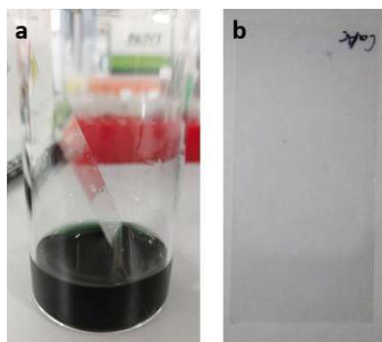


Figure 9: a) Image of the CaAc-Fe coating process of the glass slide and b) the coated glass slide

The coating was repeated another 2 times for the pre-washed glass slides and 4 times for non-washed glass slides. The glass slides were soaked in the coating solution for at least 10 min to reduce chemical consumption, by reducing the number of coating steps needed. The coated glass slides were air dried afterwards. The contact angle was measured for TA-Fe, CaAc-Fe and LS-Fe coatings on non-washed and prewashed glass slides. The concentration of the phenol and $\text{FeCl}_3 \cdot 6\text{H}_2\text{O}$ solutions can be found in Table 7.

Table 7: Concentration of Phenol and Metal-salt used for the coating of glass slides for contact angle measurement. The glass slides were put into a glass vial and combined with water, phenol- and Fe^{3+} -solution.

	c_{Phenol} (g/l) (after mixing)	$c_{\text{Metal-salt}}$ (g/l) (after mixing)
TA - Fe	0.96	0.24
CaAc - Fe	0.48	1.43
LS - Fe	1.00	1.00

To measure the static contact angle, a contact angle goniometer was used. Small water drops with a volume of $3.1 \mu\text{l}$ were dropped on the surface of the coated glass slides and pictures were taken. The contact angle was measured using a contact angle measurement tool for ImageJ software.

2.7 Hair dyeing experiments

For hair dyeing experiments brunette human hair was obtained from a volunteer. The hair was then bleached using conventional hair bleach (Schwarzkopf got 2b). After washing and drying the bleached hair was separated into different portions. For the dyeing process the hair was put into centrifuge tubes and water and a preset amount of phenol solution was added. The solution was homogenized and $\text{FeCl}_3 \cdot 6\text{H}_2\text{O}$ solution was added and it was homogenized again. After more than 10 minutes the mixture was removed and either more layers were added, or the hair

was thoroughly washed using tap water. Afterwards the hair was dried. The used concentrations were the same as in chapter 2.6 and are summed up in Table 8.

Table 8: Concentration of Phenol and Metal-salt used for the coating of human hair. The hair was combined with water, phenol- and Fe^{3+} -solution in a centrifuge tube and stayed in the solution for at least 10 minutes.

	c_{Phenol} (g/l) (after mixing)	$c_{\text{Metal-salt}}$ (g/l) (after mixing)
TA - Fe	0.96	0.24
CaAc - Fe	0.48	1.43
LS - Fe	1.00	1.00

2.8 FTIR Measurements

FTIR measurements were conducted on the raw materials to verify their structure and purity. Additional measurements were carried out with formed MPNs, if sufficient amounts were accessible. To prepare the MPNs, phenol and metal solutions were mixed, after which precipitation took place. The precipitate was washed by centrifuging and the supernatant solution was removed and replaced with water. The precipitate was then air dried for several days. Before the measurement of the sample a background spectrum (air) was taken. A small amount of the sample was crushed and put on the ATR crystal and then pressed against the crystal using the presser of the spectrometer. After the measurement the crystal was cleaned using ethanol. The measurement parameters for the IR measurements are summed up in Table 9.

Table 9: Measurement parameters used for measuring IR-spectra

Parameter	Value
Number of measurements per spectra	64
Resolution	2 cm^{-1}
Measurement Range	$400\text{-}4000 \text{ cm}^{-1}$
Apodization	Happ-Genzel
ATR-Crystal	Diamond

3 Results and Discussion

While the QCM experiments described in chapter 3.1 did not yield good results in general, UV-Vis experiments (chapter 3.2) could be used to proof MPN layer formation for TA-Fe, CaAc-Fe and LS-Fe layers. The MPN capsule formation was successful as well, and pictures of the capsules were obtained using optical microscopy, TEM, SEM and AFM. The wettability of the MPN coated glass slides was determined and the MPNs dyed hair in different colors.

3.1 QCM Experiments

QCM measurements proved to be tedious work. Due to the small size of the chips they had to be handled using tweezers. When using the N₂ stream to dry, they could be easily blown away and dropped. Furthermore, after several measurements the contact surface of the electrode exhibited signs of degradation, resulting in higher resistance values and unstable frequency measurements. Some crystals seemed to be more unstable than others, and their frequency fluctuated during measurements. The measured frequency was converted into mass change using Equation 1 (see page 6). The overall mass change for the crystal and the stepwise mass change were calculated.

The results for the MPN coating process of the QCM crystals are illustrated in Figure 10. Due to the high deviation of the measurements and to increase readability the standard error of the mean (SEM) was used for the error bars instead of the standard deviations (STD). The SEM is calculated by dividing the STD by the square root of the number of repetitions for each type of experiment (usually 3 repetitions per experiment, see Table 1).

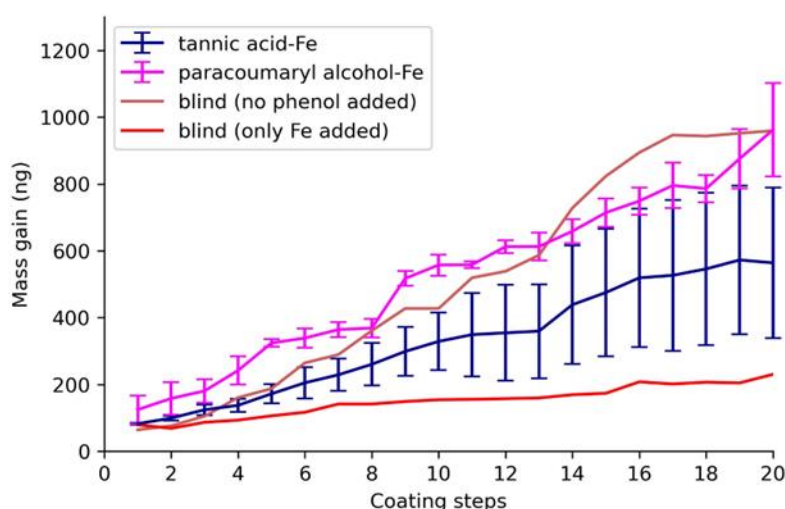


Figure 10: Total mass gain of QCM-Crystal during MPN coating process. Note: SEM was used for the errorbars instead of STD

The mass gain of the components was unstable. No definite layer growth behavior could be determined. After some steps it seemed like the growth would reach a limit, just to speed up again. The mass gain of the coating process using pCA-Fe was higher than the one of the TA-Fe process. The blind run, where only MOPS buffer and $\text{FeCl}_3 \cdot 6\text{H}_2\text{O}$ were mixed, had almost the same mass gain as the pCA-Fe coating process. The lowest mass gain was achieved with the blind process adding only Fe^{3+} solution and neither MOPS-solution nor phenol-solution.

One of the possible reasons for the high deviations of the measurements might be that the surface of the different QCM-crystals is not necessarily the same. The crystals get scratches over time changing their surface structure. Depending on the surface structure the amount of material/coating that attaches to the surface varies. The layer attached to the crystals may also be uneven or peel off, resulting in unstable measurements. Changes in air humidity or the humidity of the chip may be a problem as well.

The mass gain of the pCA-Fe coated QCM crystals is higher than the one observed for TA-Fe, which seems to be suspicious, as TA should be able to form MPNs more easily, due to the presence of vicinal diol groups [20]. Because of that, the blind measurements were performed afterwards. It was observed that, if the crystal was mixed just with water, Fe^{3+} -solution and MOPS buffer a higher mass gain could be reached, than for the trials with the addition of phenolic components. By using no MOPS buffer and just mixing with Fe^{3+} solution the mass gain was much smaller. The reason might be that the MOPS is buffered to pH 7.4 and will enhance the pH of the mixture, which results in the precipitation of non-complexed Fe^{3+} . This precipitate might attach to the crystal resulting in mass gain. To verify the possible precipitation of Fe^{3+} , 1 g/l (3.7 mmol/l) of the Fe^{3+} -salt was dissolved in the MOPS buffer used for the experiment (Figure 11). The color of the Fe^{3+} -solution in MOPS was much more intense than the aqueous solution which might indicate that a part of the Fe^{3+} precipitated.



Figure 11: 1 g/l of $\text{FeCl}_3 \cdot 6\text{H}_2\text{O}$ dissolved in 10 mmol/l MOPS and water for comparison.

According to the hydroxide precipitation diagram with the used concentration, Fe^{3+} will start precipitating above pH 2.3 [35]. MOPS buffer will increase the pH to a higher value than 2.3 and therefore lead to precipitation of Fe^{3+} . To further verify this, the coating process was mimicked by mixing 5 μl of the Fe^{3+} solution (37 mmol/l), 500 μl of water and 500 μl of MOPS buffer (20 mmol/l) and the mixture was centrifuged afterwards. The same process was repeated using water instead of MOPS buffer. In the solution containing MOPS, orange precipitate was visible at the bottom. This could explain the higher mass gain of the pCA-Fe coating experiment since the complexation of Fe^{3+} by pCA is probably much weaker than the complexation of Fe^{3+} by TA and hence more Fe^{3+} might be available to be precipitated and attach to the MPN crystal surface.

Due to the high error of the measurements as well as the mass gain without using phenols this experiment was stopped and not performed with the other phenolic compounds.

The dipping process was performed for all phenolic components except for CaAc. Just like the other QCM coating process the dipping process has some mass gain even without the usage of phenolic compounds (Table 10, blind). To calculate the values in the table, outliers were eliminated after visual inspection of the data. The data did not seem to be normally distributed in some cases and included outliers at both ends, making other outlier detection methods unusable. In this process the MOPS-buffer and the Fe^{3+} -solution did not get in direct contact, therefore Fe^{3+} precipitation should not occur as in the previous coating process.

Table 10: Measured average mass gain after the dipping steps for different MPNs during the dipping process.

	TA-Fe	pCA-Fe	CA-Fe	SA -Fe	LS - Fe	blind
Avg. Mass gain after dipping in Phenol (ng)	87	117	28	28	30	10
Stdv. Mass gain after dipping in Phenol (ng)	28	43	26	26	23	17
Avg. Mass gain after dipping in Fe (ng)	22	25	28	14	40	31
Stddv. Mass gain after dipping in Fe (ng)	16	23	30	30	30	24

The error range for the coating process using dipping is still big, hence SEM was used for error bars to illustrate the results and increase readability of the graphs (Figure 12).

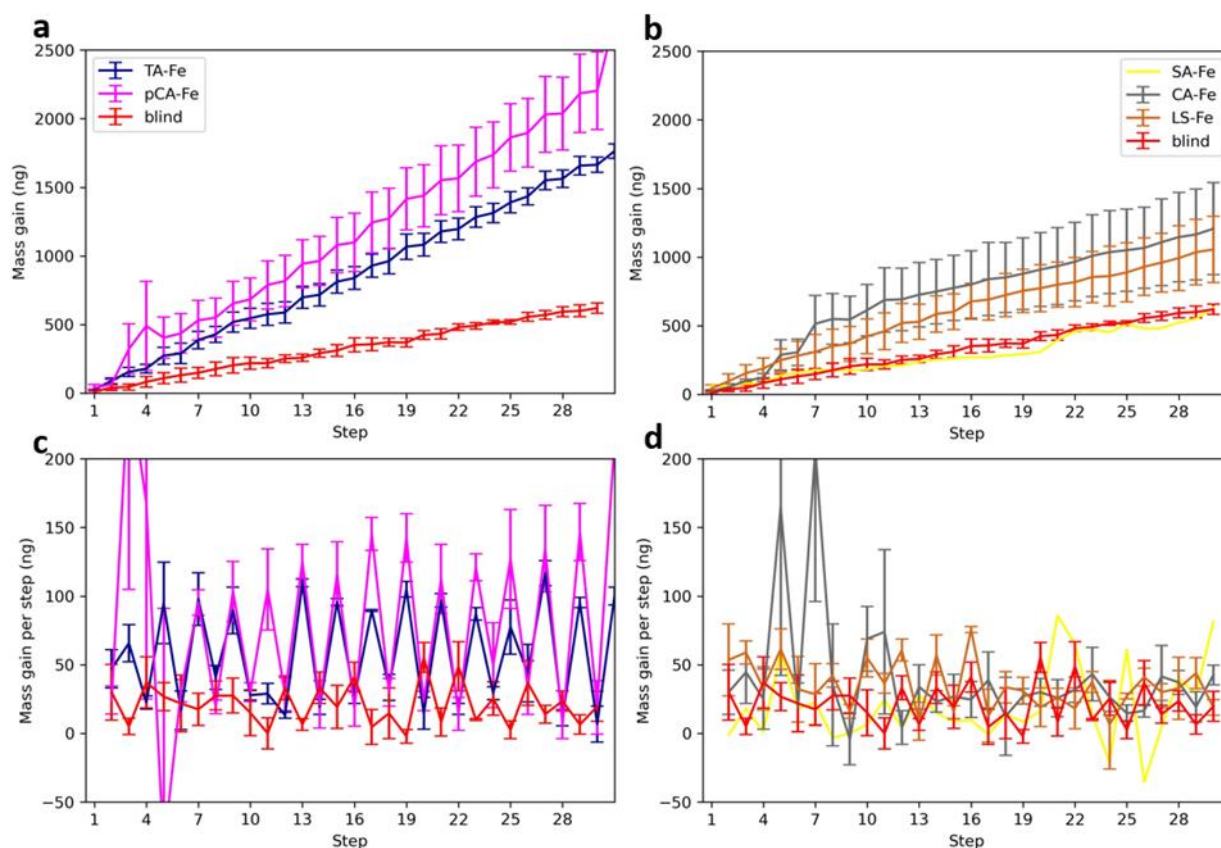


Figure 12: Results for the mass gain of the MPN coating process using the dipping method. The upper diagrams (a,b) illustrate the total mass gain for all steps. The lower pictures (c,d) depict the stepwise mass gain. The errorbars were generated using SEM instead of STD to increase readability of the diagrams. a,c) TA-Fe and pCA-Fe, b,d) SA-Fe, CA-Fe and LS-Fe

For TA and pCA a ladder like, stepwise mass gain can be seen. The mass gain is bigger after dipping into phenolic solution, than after dipping into Fe^{3+} solution. Reasons might be that the mass of the attached Fe^{3+} is smaller than the one of the phenolic compounds or that the MPN-layer is partially degraded because the pH of the Fe^{3+} solution is at 2.7. The experiments suggest that TA and pCA can form MPN layers. For SA no mass gain, exceeding the blind mass gain, could be observed. Therefore, SA was only examined once. A slightly bigger mass gain for CA and LS than with the blind was observed. However, the error range is big and overlapping with the mass gain of the blind indicating no significant difference.

In 1 of the 3 dipping experiments with pCA the formation of various blue spots on the QCM crystal was observed as seen in Figure 13. This indicates that the pCA-Fe layer formation may be uneven and instead of the formation of a continuous layer the pCA-Fe MPN attaches only at some spots of the crystal.



Figure 13: QCM crystal consecutively dipped into paracoumaryl alcohol and iron solution with blue spots on the surface.

The last experiments performed using the QCM were the disassembly experiments at pH 2, 3 and 5 and in EDTA solution. The results for the disassembly experiments at pH 5 as well as the result for the disassembly experiment of the LS-Fe MPN at pH 3 exhibited mass gain instead of a mass loss (Appendix, Figure 45). The disassembly experiments for pCA-Fe at pH 3 and pH 2 and in EDTA as well as the disassembly experiment using LS-Fe in EDTA had mass loss as expected (Figure 14).

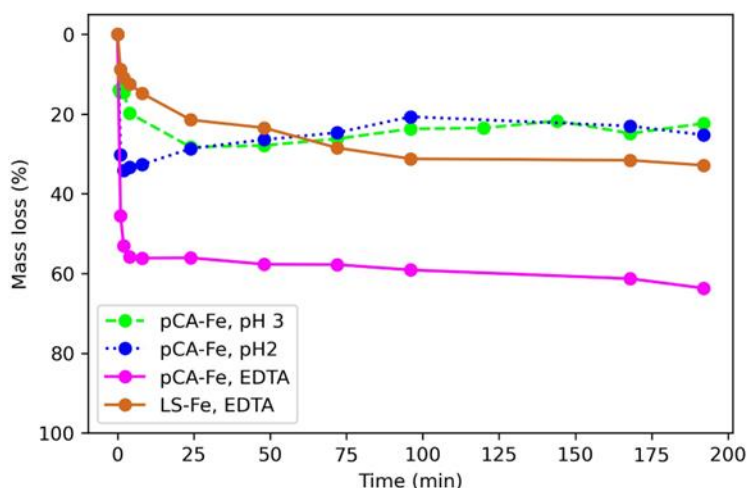


Figure 14: Disassembly of MPN coatings on QCM crystals at different conditions. The starting mass before the disassembly was between 1026 ng and 1448 ng

A steady mass loss can be observed for the disassembly experiments using EDTA solution. For no experiment a total disassembly of the coated layer could be observed, and the maximum mass loss was reached for the pCA-Fe layer disassembled in EDTA. For the disassembly experiment of the pCA MPN at pH 2 the mass started to increase again after 2 minutes. To prevent mass gain by attachment of other compounds dissolved in the solution the pH of the disassembly solutions was set using HCl and no additional buffer. Still a mass gain was observed.

It remains unknown what might cause this mass gain. Possible reasons are the attachment of dust or humidity remaining on the QCM crystal after drying with the N_2 -stream. Due to the poor robustness and repeatability of the QCM measurements, UV-Vis measurements were performed instead of further QCM-measurements.

3.2 UV-Vis experiments

For SA-Fe and CA-Fe no LMCT band could be observed and neither color change when mixing the phenol and Fe^{3+} solution nor the development of bands in intensity in the UV-Vis absorption region was visible. Since these components did not indicate promising results in the QCM-experiments either, no further experiments were conducted. For pCA-Fe a slight color change of the solution towards blue was observed and a small LMCT band at 600 nm was visible (Appendix, Figure 47). The TA-Fe solution had an intense blue color and CaAc-Fe solutions were strongly green. For LS-Fe the light brown color of the solutions intensified after mixing and visible precipitation was observed after a few seconds.

The mixing of CaAc solution and Fe solution in different ratios demonstrated that the color intensity of the complex is the strongest when a CaAc:Fe molar ratio of 1:1 or 1:2 is used, as can be seen in Figure 15. Some water was added after taking the first picture to reduce the absorption and enable UV-Vis measurements. After some time, precipitation occurred, resulting in the discoloration of the solution. No precipitation was observed for a CaAc:Fe ratio of 4:1 and only slight precipitation occurred at a ratio of 2:1. All solutions with a CaAc:Fe ratio of 1:1 and below exhibited strong precipitation.

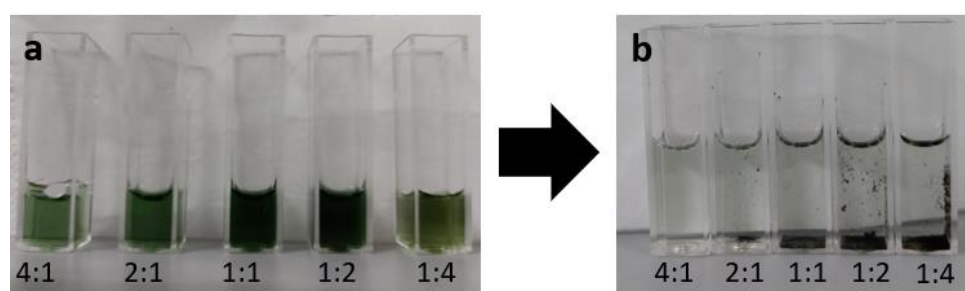


Figure 15: Caffeic Acid and Iron mixed in different molar ratios. a) directly after mixing, b) after one day

When mixing the LS and $FeCl_3 \cdot 6H_2O$ in different mass ratios the color seemed to be most intense at a ratio of 2:1 (see Figure 16). However, no precipitation occurred at this ratio. The

solutions had to be diluted with water to measure UV-Vis spectra. Precipitation was found in mass ratios of 1:1 and below with the strongest precipitation at a ratio of 1:1.

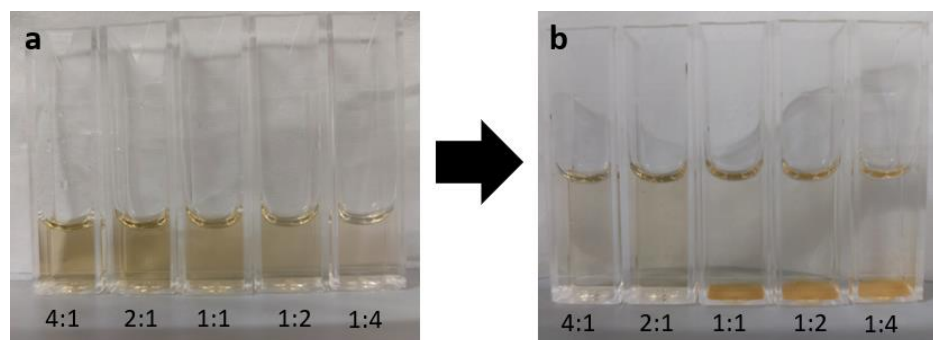


Figure 16: Lignosulfonate and $\text{FeCl}_3 \cdot 6\text{H}_2\text{O}$ solution mixed in different mass ratios. a) directly after mixing, b) after one day

UV-Vis spectra of the Phe:Fe mixtures at different ratios were measured and the intensity of the absorption at a chosen wavelength was used to predict the best ratio for MPN coating (see Figure 17). The LMCT band position for CaAc-Fe and pCA-Fe were chosen for evaluation (650 and 600 nm respectively) and 570 nm for LS-Fe, because the absorption of mutual LS is weak at this wavelength. The absorption of CaAc-Fe is the strongest at a molar ratio of 1:2 which is in accordance with visible observations. The average molar mass of LS is unknown hence the mass ratio of the LS and $\text{FeCl}_3 \cdot 6\text{H}_2\text{O}$ was used instead. For LS-Fe the highest absorption is reached at a mass ratio of 1:1 which is also the ratio with the most observed precipitation. To receive the mass ratio of LS: Fe^{3+} (the mass ratio of LS: $\text{FeCl}_3 \cdot 6\text{H}_2\text{O}$ is given) a correction factor of 4.84 can be used. A mass ratio of 1:1 LS: $\text{FeCl}_3 \cdot 6\text{H}_2\text{O}$ corresponds to a ratio of 4.84:1 LS:Fe accordingly. The LS:Fe ratio of 4.84:1 exhibited the most precipitation and is very close to the maximal complexing capacity of LS and Fe^{3+} found in literature, which corresponds to an LS:Fe ratio of 4.4:1 to 3.1:1, depending on the type of LS used [36]. The pCA-Fe mixtures showed a band at 600 nm and the absorption was by far the highest at a molar ratio of 1:1.

One of the problems of this method is that the absorption spectra of the mixtures strongly change with time. This is probably due to the occurring precipitation and the precipitated particles influencing the UV-Vis measurement. On the one hand, if precipitated complexes are in the measurement path, the observed absorption may increase. On the other hand, the precipitation removes dissolved complexes from the solution, resulting in a decrease of absorption. Another method to optimize the Phe:Fe ratio would be to wash the cuvettes after letting the solution sit in the cuvettes for some time. Then the cuvettes could be filled with water again and spectra of the layer formed on the cuvette wall could be obtained. However, it may be necessary to repeat this coating process with the different ratios multiple times since the

3 Results and Discussion

absorption of one layer is usually very weak and difficult to observe. Still, the used method was easy, and timesaving and the obtained data was consistent with the results from the MPN-capsule experiments.

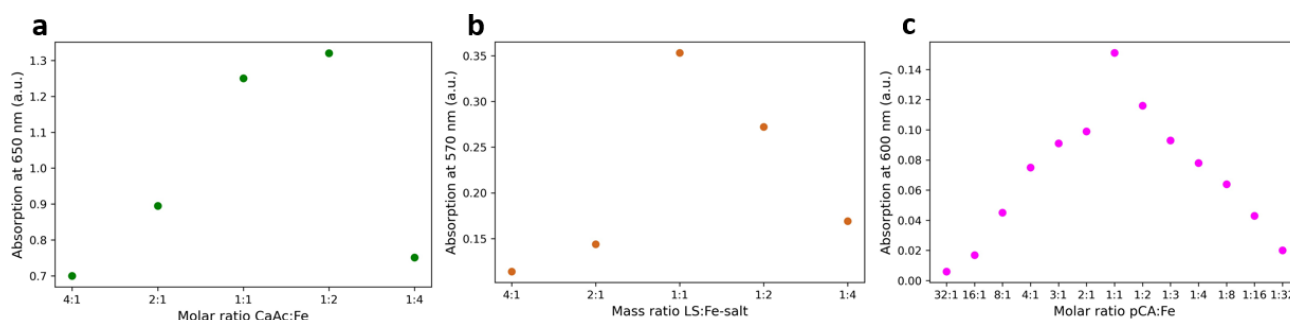


Figure 17: UV-Vis data for optimization of the Phe:Fe ratio. Phenol and Iron-solution were mixed in different ratios and diluted with water. a) Results for CaAc-Fe at 650 nm (absorption maximum of LMCT band), b) results for LS-Fe, note the mass ratio of the lignosulfonate and Iron-salt is depicted, c) results for pCA-Fe at 600 nm (absorption maximum of LMCT band)

Since the CaAc-Fe complex exhibited an intense green color, the next point of interest was the behavior of the complex at different pH-values. Mixing CaAc and Fe^{3+} solutions and adjusting the pH resulted in a broad range of colors. The color of the CaAc-Fe solution is strongly dependent on the pH-value. At a pH of 1 the complex is almost colorless with a slight yellow tone (see Figure 18). At pH 3 and pH 4 the complex is green and turns to a greenish grey at a pH of 5 to pH 6. At pH 7 and pH 8 the solution is grey and at a pH of 9 and above the solution is brown red. After waiting for 3 days precipitation is visible from pH 3 to pH 6.

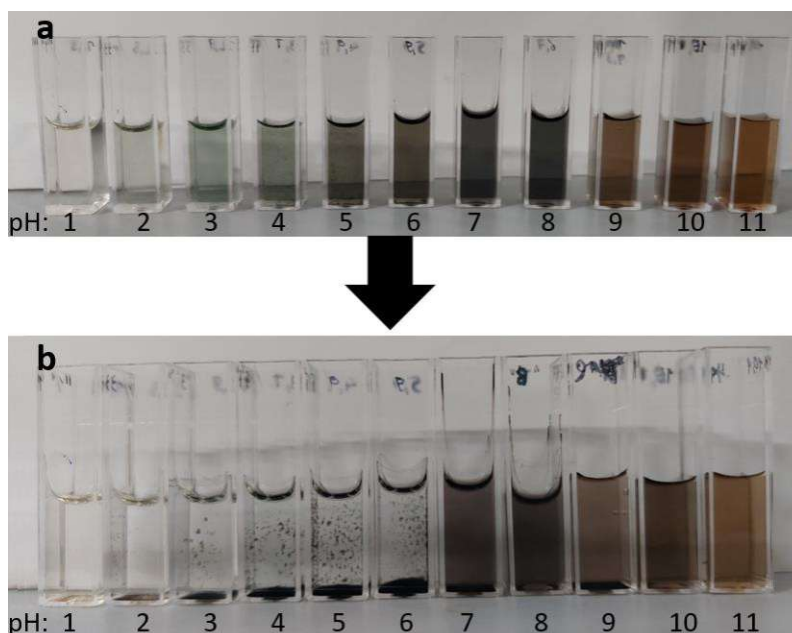


Figure 18: Image of the CaAc-Fe complex at different pH. a) Image taken right after mixing the components and adjusting the pH, b) Image taken after 3 days

The obtained absorption spectra from the fresh CaAc-Fe solutions at different pH and the layers built on the cuvette walls after some days exhibit strong difference in CaAc-Fe complexation depending on the pH (see Figure 19).

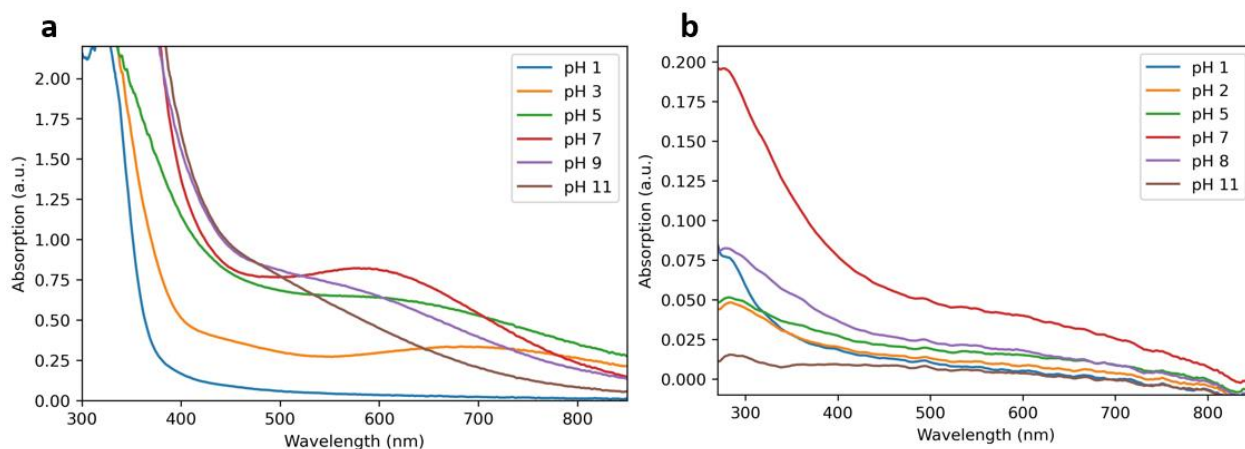


Figure 19: Absorption spectra of the (a) Ca-Fe complex solution directly after mixing and b) of the CaAc-Fe layer formed on the cuvette walls after one week.

At pH 1 no absorption occurs at wavelengths above 380 nm and no LMCT band is visible. At pH 3 the LMCT band is visible with a maximum at 700 nm. As the pH increases the LMCT band shifts to smaller wavelengths. At pH 7 and pH 8 the maximum is at 580 nm. At pH 9 and above the LMCT band is either not apparent anymore or merged with the absorption band at smaller wavelengths. A layer formation with absorption at wavelengths above 450 nm could be observed from pH 3 to pH 8. At higher pH no layer formation was present at the cuvette walls and at lower pH absorption could only be observed at smaller wavelengths.

This pH dependent changes in color of the complex are similar to the behavior reported for TA-Fe and Catechol-Fe complexes [5,37]. The formation of mono-, bis- and tris-complexes is pH dependent, and the color of the solution is influenced accordingly. At low pH most of the hydroxyl-groups of CaAc are protonated and the mono-complex is most common. At higher pH-values the bis-complex is formed. At high pH > 7 tris-complexes are predominantly formed. This change can be observed in the shift of the LMCT band. The higher the pH the lower the wavelength of the observed LMCT band was. Since precipitation occurred from pH 3 to pH 8, it can be concluded that the bis-complex may be necessary for MPN layer formation. Another reason why no layer is formed at high pH may be, that CaAc is not stable at high pH and the phenol group gets oxidized to quinone [38].

Mixing CaAc and LS-solutions with Mn^{2+} , Al^{3+} , Cu^{2+} and Co^{2+} , no color change or precipitation was visible. The combination of CaAc-solution and Zr^{4+} -solution resulted in a green-yellow

solution (see Figure 20). After some time, precipitation took place and by centrifuging green-yellow precipitate was yielded. The combination of the LS and Zr^{4+} solutions resulted in the formation of light-brown precipitate. These results indicate that MPN formation is probably possible using Zr^{4+} as metal ion and LS and CaAc as ligand.

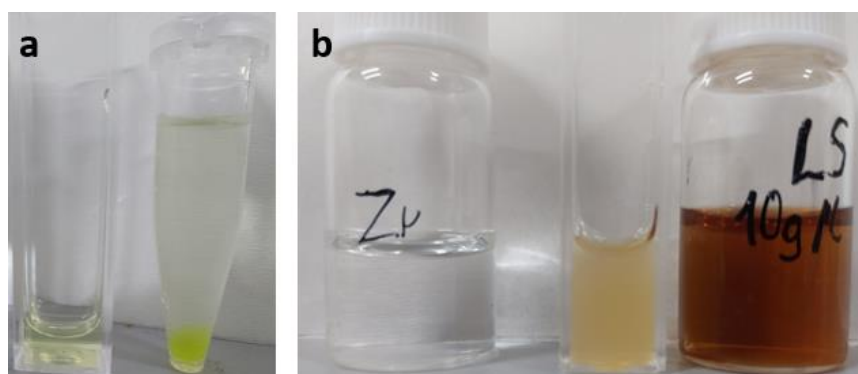


Figure 20: a) Image of mixture of CaAc and Fe-solution and precipitate after centrifugation, b) Mixture of LS and Zr-solution and color of the mutual solutions for comparison

For the first coating experiments of cuvettes, one-time coated cuvettes after removing the water were used as background. This resulted in unstable results for the layer growth because a different amount of water attached to the walls of the cuvette during the measurement every time. Because of that, a clean cuvette filled with water was used as background later and the coated cuvettes were filled with water before the measurement as described in paragraph 2.4.4. This yielded more stable results, especially when the layer build-up was relatively small. Spectra of the MPN-coatings as well as pictures of the coated cuvettes can be seen in Figure 21.

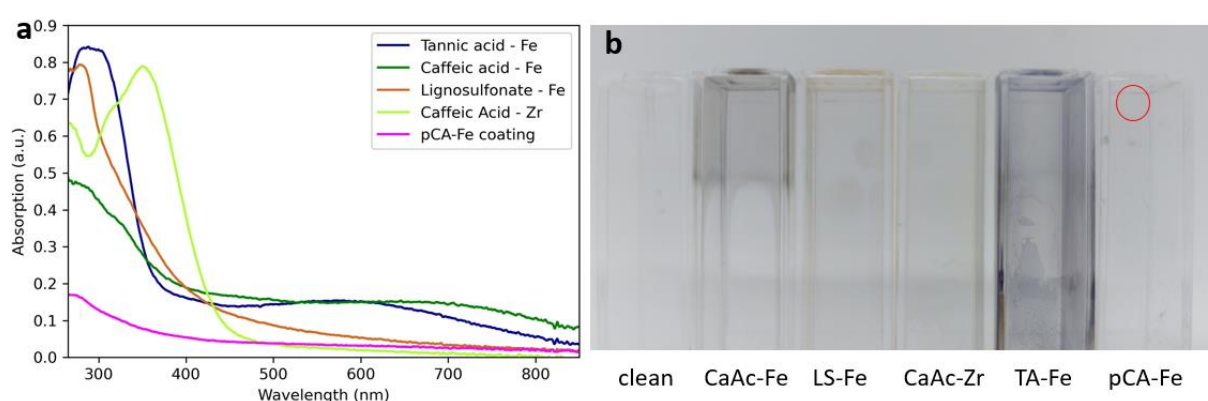


Figure 21: a) Absorption Spectra of the MPN coated cuvettes and b) images of coated cuvettes demonstrating the color of the coating. In the red circle a blue spot of pCA - Fe MPN is visible but no continuous coating was formed. For the formation of the pCA-Fe layer iron solution and buffered pCA solution were put into the cuvette in succession.

The TA-Fe film exhibited a broad spectrum with an absorption maximum at 295 nm. In accordance with literature a broad ligand-to-metal charge transfer (LMCT) band at ~570 nm

was observed [5]. The color of the film was blue. The absorption maximum of the CaAc-Fe film is estimated to be at ~ 250 nm. Due to the wavelength limitation of acrylic cuvettes, it can only be estimated. A broad LMCT band was observed at 650 nm. The LS-Fe film exhibited an absorption maximum at 280 nm and no LMCT band was observed in the range from 400 nm to 800 nm. The film color was orange. The CaAc-Zr film had two absorption maxima, with one maximum below the measurement range and another maximum at 350 nm and a neon yellow color. The build-up of the LS-Zr layer failed. For pCA-Fe no layer build-up was visible at first. Only after using the dipping process used for the coating of the QCM crystal, but with flexible dipping time, some change was visible. However, the absorption of the pCA-Fe coating was much weaker than the one of the other coated cuvettes. Furthermore, it was found that no continuous layer was built, but a few blue spots attached to the cuvette walls. This is consistent with the observations made during the dipping process of the QCM crystals.

For the interpretation of the results, it was assumed that the Lambert-Beer Law (Equation 2) does apply to the measurements. Hence it was concluded that the absorption of the layer directly correlates with the layer thickness. Note that this may not necessarily be true, as the absorption was below 0.1 in some cases, and the Lambert-Beer law is not considered generally applicable at absorption below 0.1 and above 1.2. Furthermore, the structure of the MPNs may change, causing a different absorption coefficient and therefore a change in absorption. This was for example the case for the disassembly of TA-Fe in MOPS buffer (results and discussion below)

Multistep layer coating on cuvettes worked well for TA-Fe, CaAc-Fe and LS-Fe. The layer absorption increases linearly with the number of layers (see Figure 22). For the TA-Fe layer a strong concentration dependence was found. Increasing the TA concentration (and the Fe concentration respectively) from 0.24 g/l to 0.48 g/l increases the intensity of the layer coating process threefold. Increasing the concentration again from 0.48 g/l to 0.96 g/l results in another rise by three times of the intensity. At a TA concentration of 4 g/l for the stepwise assembly of TA-Fe layers the absorption limit of the UV-Vis spectrophotometer is nearly reached, demonstrating one of the limitations of using UV-Vis spectroscopy to monitor layer formation. In the chosen concentration range for CaAc-Fe a linear dependence between concentration and layer absorption was found. In contrast, the LS concentration did not influence the absorption of the layer strongly. In the concentration range of 1 g/l to 2 g/l of LS no concentration dependence was found. Lowering the LS concentration to 0.5 g/l only resulted in a slight reduction of the layer build-up.

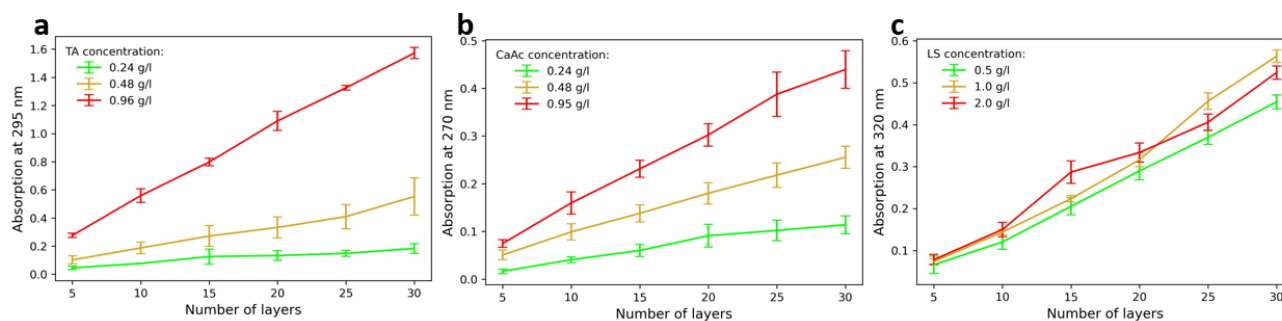


Figure 22: Multistep MPN layer build up monitored using UV-Vis. The ratio of phenol to iron was kept constant for all experiments. a) TA-Fe, b) CaAc-Fe c) LS-Fe

A continuous layer-build up on the cuvette walls could be confirmed for CaAc-Zr (see Figure 23). However, no layer was formed on the cuvette walls using LS-Zr. It could be that the ratio of LS:Zr would need adjustment to successfully form MPN coatings or the precipitation takes place too fast in the solution and not on the walls of the cuvette.

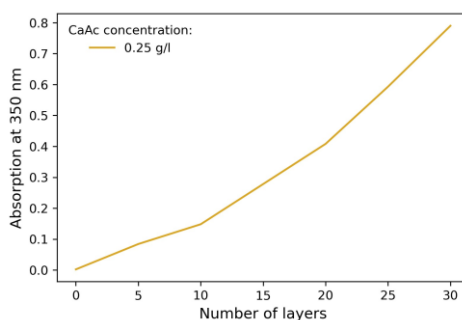


Figure 23: Layer build-up of the CaAc-Zr layer, monitored using UV-Vis spectroscopy.

The time-dependence of the coating process was monitored using UV-Vis spectroscopy. The results are illustrated in Figure 24. For TA-Fe no specific behavior for the coating process over time was found. The layer seems to form rapidly, and then no definite trend was observed for the first 4 hours. After 20 hours the absorbance at 295 nm increased significantly to 0.084 to 0.144 for the three attempts. The same behavior was found for CaAc-Fe, the layer forms rapidly within 10 min and afterwards no definite trend is visible. After 19-20.5 hours the absorption at 270 nm increased considerably and was above 0.1 for all three attempts. The LS-Fe exhibited much more steady results. The coating is rapid in the beginning and seems to slow down afterwards.

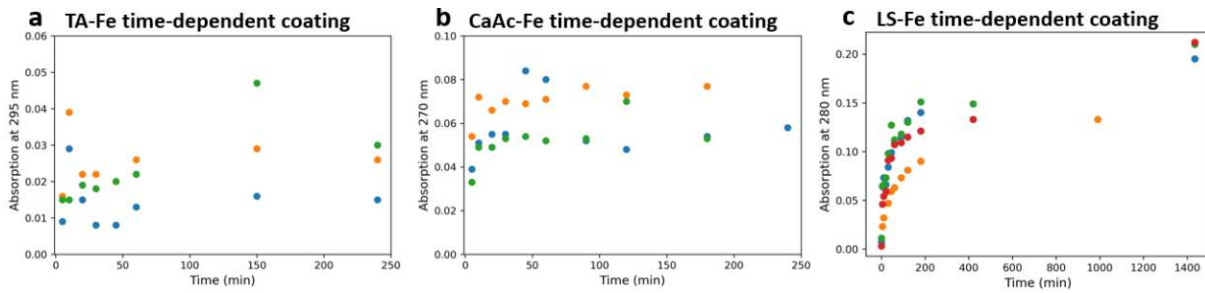


Figure 24: Time dependence of the MPN coating process. a) TA-Fe coating, b) CaAc-Fe coating, c) LS-Fe coating

The results for TA-Fe do not agree with the results found by Yun et al. [24] which predict an assembly behavior like the one observed for LS-Fe. One reason for the strong increase in layer formation after long periods of time but no tendency in the beginning may be that the measurement process itself disrupts the formation of the layer, because the coating solution is temporarily removed from the cuvette and the cuvette is spilled with water.

The disassembly of the MPN coated cuvettes in different conditions was examined for TA-Fe, CaAc-Fe and LS-Fe using UV-Vis spectrophotometry. The cuvettes were coated till they had roughly the same absorption intensity. The absorption at 320 nm in the beginning was roughly 0.6, 0.3 and 0.5 for the TA-Fe, CaAc-Fe and LS-Fe coatings respectively. To demonstrate the percentage of disassembled layers, the absorption at the beginning was used to scale the data by dividing all datapoints with the absorption in the beginning. The results are illustrated in Figure 25 (for a closer view of the disassembly in the first 2 hours, see Appendix, Figure 48).

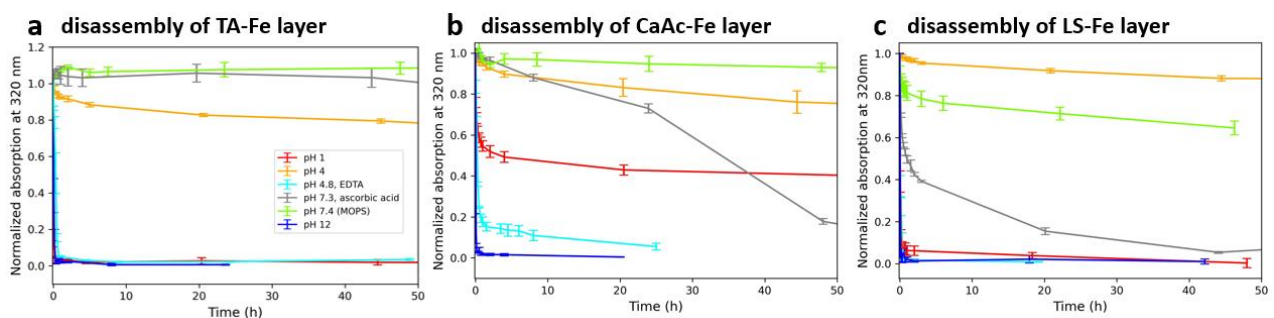


Figure 25: Disassembly of the MPN layers at different conditions, monitored by UV-Vis spectrophotometry. a) disassembly of the TA-Fe layer, b) disassembly of the CaAc-layer, c) disassembly of the LS-Fe layer

The TA-Fe film is the most stable at pH 7.4 and displays no decrease in absorption. Even after 95 h the absorption does not decrease considerably. The shape of the absorption spectrum changes, as can be seen in Figure 26. The film slowly degrades at pH 4 and rapidly degrades at pH 1, pH 2 and in EDTA (10 mmol/l). After 5 min 90 % of the absorption at 320 nm is lost at pH 1. At pH 12 it takes 10 min to decrease the absorption by 90 % and in EDTA (10 mmol/l)

it takes 30 min. The sodium ascorbate solution (10 mmol/l) does not seem to degrade the film in the first 24 hours. However, after waiting some more time, the film begins to degrade.

The behavior of the CaAc-Fe film is similar to the one of the TA-Fe film. The CaAc film is the most stable at pH 7.4 and even after 70 h more than 90 % of the absorption remains. It slowly degrades at pH 4 and rapidly degrades at pH 1, pH 2 and in 10 mmol/l EDTA. At pH 1 part of the absorption at 320 nm remains (see Figure 27). Like TA-Fe there is a set off time for the CaAc-Fe layer, till the disassembly by the sodium ascorbate begins. In the first 2 hours no disassembly takes place and 97 % of the absorption remains. After 2 hours the layer starts to disassemble and after 71 hours and 45 min only 3 % of the absorption at 320 nm remains.

The LS-Fe films disassembly behavior is different from the behavior of the other films. It is the most stable at pH 4 and 87 % of the initial absorption remains after 68 h. It quickly partially disassembles at pH 7.4 and 20 % of the absorption is lost after the first 45 min and after 46 h 40 % of it is lost. The film is not stable in pH 1, pH 12 and EDTA solution (10 mmol/l). More than 90 % of the absorption intensity at 320 nm is lost after 5 min at pH 12 and after 20 min at pH 1. In EDTA it takes 30 min to decrease the absorption intensity by 90 %. The disassembly in sodium ascorbate (10 mmol/l) starts immediately, and after 44 h less than 3 % of the absorption remains.

One of the limitations of this method is that UV-Vis absorbing disassembly solutions disturb the measurement. The sodium ascorbate solution absorbs at wavelengths below 320 nm which is why the results were evaluated for the absorption at 320 nm. This problem could be circumvented by filling the cuvette with water for the measurement. However, this will decrease the accuracy of the disassembly time because the cuvette is filled with water for longer time periods.

All MPN films were disassembled in EDTA solution. It can be concluded that competitive chelation occurs and the binding affinity of the EDTA is higher than the one of the phenols. This means the films were built through coordinative bonding between Fe^{3+} and the Phenols as expected and not through precipitation due to changed solution conditions (low pH, ionic strength etc.). Acidic pH disassembled the coating too, as it led to the formation of mono-complexes, which are not able to form networks. At high pH values TA and CaAc are not stable and are oxidized, probably leading to a disassembly of the MPN layer [38,39]. The disassembly of MPNs by sodium ascorbate is probably caused by reduction of Fe^{3+} to Fe^{2+} . The slow speed of the process could be explained by the neutral pH of the disassembly solution as the reduction

potential of the Phe-Fe complexes decreases at higher pH values [40]. The different disassembly behavior of the LS-Fe coating could be caused by the different functional groups involved in the coordinative bonding.

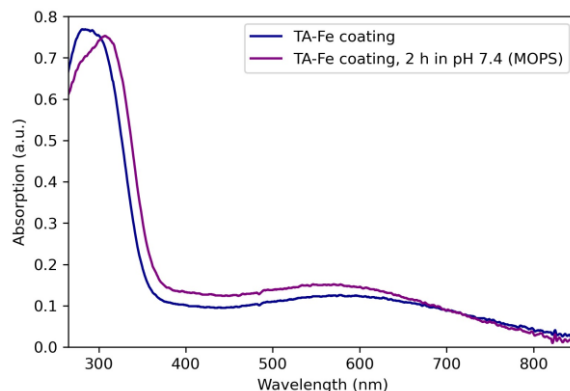


Figure 26: Change of the UV-Vis absorption spectrum of TA-Fe after 2 h in pH 7.4 MOPS solution

At pH 7.4 (MOPS buffered) the absorption maxima of the TA-Fe film shifted causing the layer to change color towards purple. It was seen that after 2 days at some parts of the cuvette, flakes of the TA-Fe coating peeled off the wall. The more intense absorption maximum shifts from 295 nm to 307 nm and the maximum of the LMCT band shifts from 577 nm to 570 nm. This pH-dependent behavior of TA-Fe complexes has been reported in literature [5] and may be caused by the change between bis- and tris-complexes.

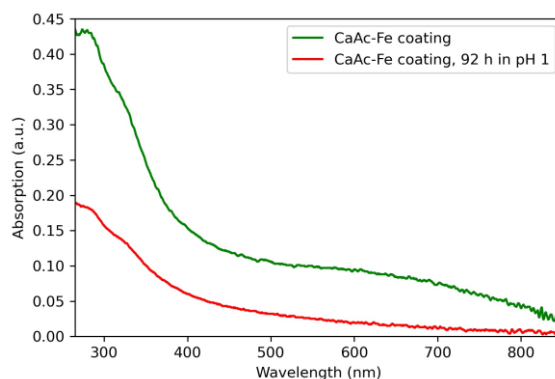


Figure 27: Change of the UV-Vis absorption spectrum of CaAc-Fe after 92 h in pH 1 solution

After disassembly in pH 1 solution for 92 h the absorption spectrum of the CaAc-Fe layer changes significantly. While the LMCT band at 600 nm disappears almost completely, 40 % of the absorption at 320 nm remains. The green color of the layer is not visible anymore and it seems that the layer was totally degraded. It is unclear what causes this remaining absorption. Fe^{3+} is soluble at pH 1 and does most likely not cause the remaining absorption, as this behavior

was not found for the disassembly of the TA-Fe and LS-Fe coating at pH 1. This indicates the absorption can only be caused by CaAc or some compounds formed by CaAc.

3.3 MPN Capsules

MPN capsules were assembled successfully under different conditions. In Figure 28 pictures were taken after the major steps of the coating process. The addition of phenol and Fe^{3+} results in a color change of the mixture. After washing with water, the coated PS-spheres remain, and unreacted phenol and Fe^{3+} are removed. Depending on the success of the capsule formation, the color of the PS-spheres changed from white to the color of the MPNs. Additional complex precipitation was visible in that step and sometimes an extra layer of precipitate could be seen on top of the capsules. After washing with THF only the hollow capsules remained, and the PS was dissolved. The number of visible remnants indicated the success of the process. If no visible remnants remained, it usually meant the process had failed. In contrast, big amounts of remnants could also lead to the result, that a lot of extra complex debris was formed instead of or additionally to the capsules. The coating process was varied in different ways, for example by exchanging the MOPS solution with water, using less PS particles, or more phenol- and Fe^{3+} -solution instead of water. It was found that MOPS solution is not necessary for capsule stabilization. Using less PS particles did not influence the process considerably.

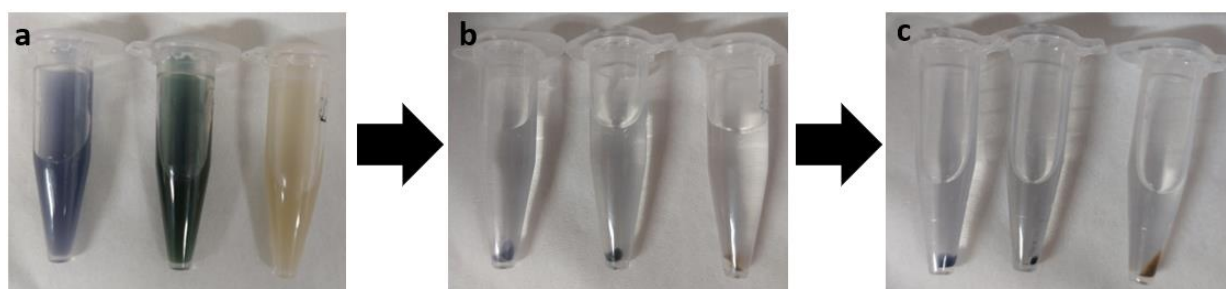


Figure 28: Capsule preparation of TA-Fe, CaAc-Fe and LS-Fe capsules (left to right in each picture). a) After addition of the reagent the color of the solution changes, b) excess reagents are removed by washing with water c) the PS-spheres are dissolved in THF, and the capsules remain.

One of the factors that seemed to be of great importance to capsule formation, was the Phe:Fe ratio. For TA-Fe complexes a ratio of 1:1.6 was chosen, as this ratio was known to work for MPN formation [24]. For CaAc-Fe the ratio was adjusted to 1:2 as this was found to be the best ratio in the UV-Vis experiments. A ratio of 3:2 was tested in the beginning, but no capsules were formed, and a lot of green precipitate was formed instead. For CaAc concentrations of 1 g/l the capsules tended to aggregate. By using smaller CaAc concentrations the aggregation was minimized. Since layer formation for CaAc-Fe should be stronger at neutral pH a small

amount of NaOH was added in one capsule formation attempt. This did not lead to better capsule quality and quantity, but a lot more complex precipitate was formed instead. For the formation of LS-Fe capsules a mass ratio of 2:1 (LS:FeCl₃·6H₂O) or smaller was found to be necessary for capsule formation. Attempts using a mass ratio of 4:1 failed. Multiple attempts of forming CaAc-Zr, LS-Zr and pCA-Fe capsules failed, and capsules could not be retrieved. One problem of the capsule formation with pCA-Fe was, that after the chemicals were added, the PS-spheres would not completely settle anymore using centrifugation and some spheres would keep on floating in the supernatant solution. It was suspected that a change in zeta-potential might be the cause of the problem and NaCl was added to try to adjust the zeta-potential. This did not resolve the problem though and increased the density of the solution which made it even more difficult to settle the microspheres through centrifugation. In another attempt, it was tried to add some NaOH to adjust the pH and achieve capsule formation. This didn't work either. A table with all attempted capsule experiments including the result of each experiment can be found in the Appendix (Table 12).

For TA-Fe and CaAc-Fe smooth capsules were retrieved. Most of the capsules were intact and the amount of debris in the solution was small (Figure 30). The percentage of damaged capsules seemed to be small. The SEM and TEM pictures show the capsules. The folds and creases are formed because the capsules collapse when the surrounding solution evaporates. LS-Fe capsules were not smooth, and some debris was attached to them. They had a much lower mechanical stability and most of the capsules in the solution were broken (Figure 29). Great care had to be taken to keep the mechanical strain during the washing step as low as possible and fewer washing steps were executed. A lot of debris was present in the LS-Fe capsule solution. Using SEM, only unsatisfying images of the capsules could be obtained, due to the big amount of debris overlapping with the capsules. One approach to receive smoother capsules and less debris could be to first mix the phenol and Fe³⁺ solution, then filter the solution to remove the precipitate and mix the filtered coating solution with the PS-microspheres to coat them.

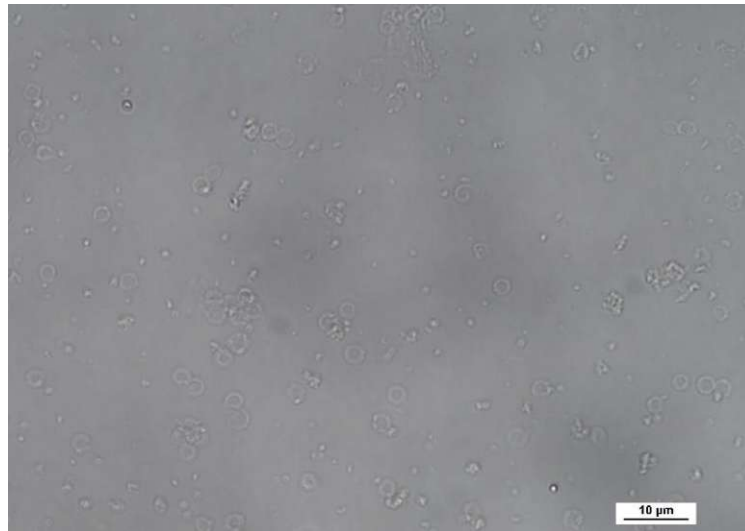


Figure 29: Optical microscope image of LS-Fe capsules. Broken capsules and debris are visible.

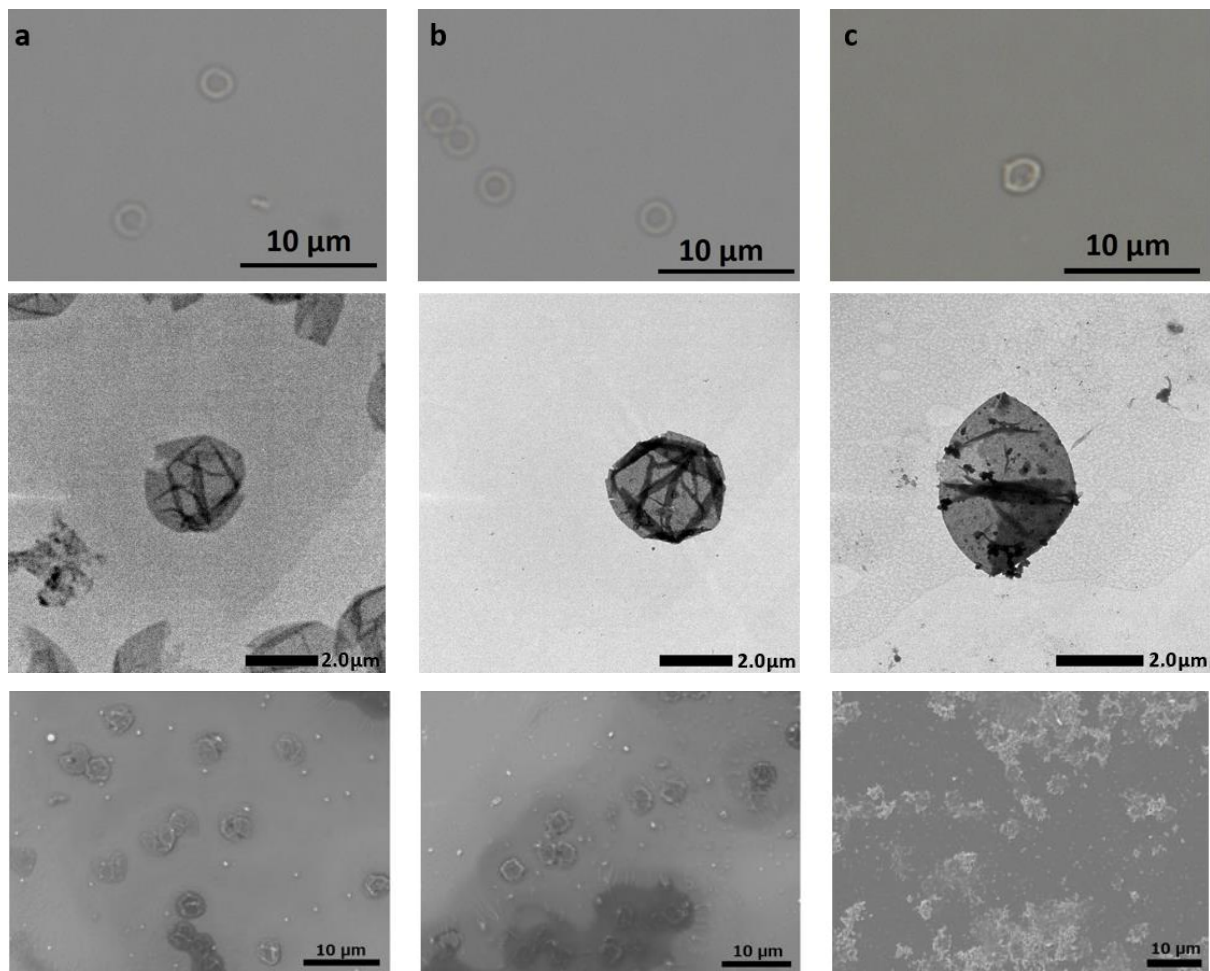


Figure 30: Optical microscope, TEM, and SEM pictures of a) TA-Fe, b) CaAc-Fe and c) LS-Fe capsules.

Elemental analysis was performed using the SEM by dropping a concentrated capsule solution on the silicon wafer. Single capsules couldn't be analyzed because the layer thickness of the capsules is too small. The EDS-Spectrum of the TA-Fe capsules (Figure 31) has a strong Si-K α

line, which suggests that the layer of the TA-Fe capsule film was not thick enough and the silicon wafer below the sample was partially sampled. Weak C-K α , O-K α and very weak Fe-L α lines are visible as well. Hence all the elemental components of the TA-Fe film could be verified (except for hydrogen which is not measurable using EDS analysis).

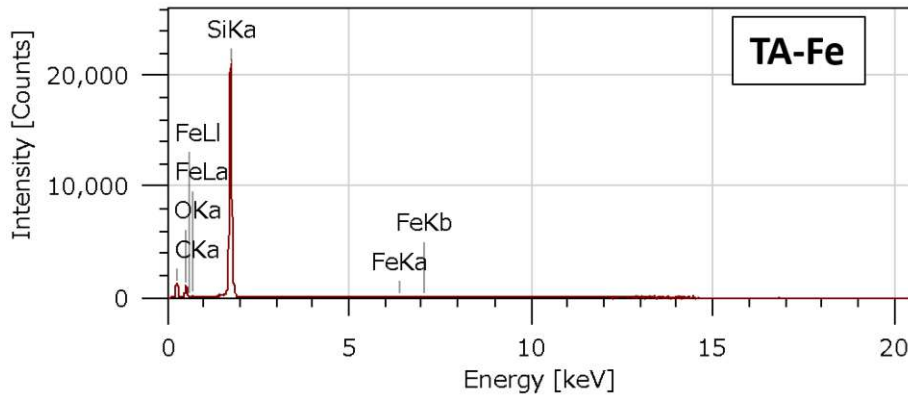


Figure 31: EDS spectrum of the TA-Fe capsules

The EDS spectrum of CaAc-Fe (Figure 32) shows the same results as TA-Fe because the elements present in the CaAc-Fe coating are the same as in TA-Fe. The Si-K α line is a bit weaker and the C-K α , O-K α and Fe-L α lines are stronger. The Fe-K α line is visible as well.

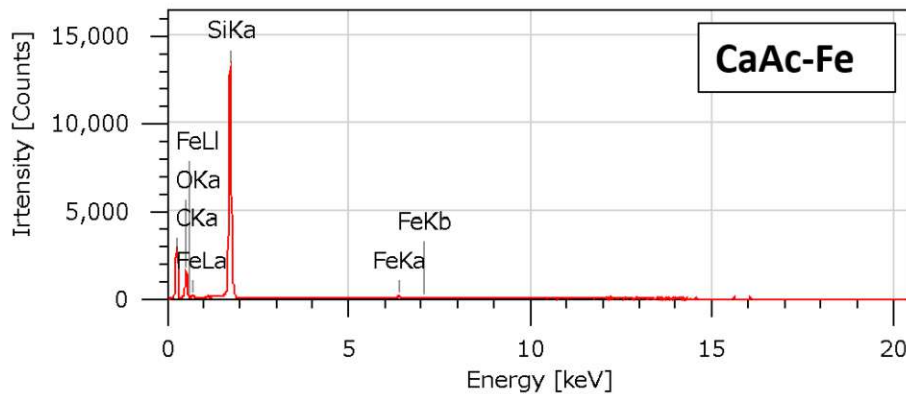


Figure 32: EDS spectrum of the CaAc-Fe capsules

The EDS-spectrum of LS-Fe (Figure 33) shows bands for all expected elements. C-K α , O-K α , S-K α , Fe-L α , Fe-K α and Fe-K β lines can be seen and the intensity of the Si-K α line is low. This indicates that the LS-Fe capsule layer is thick enough to not measure as much signal from the silicon below.

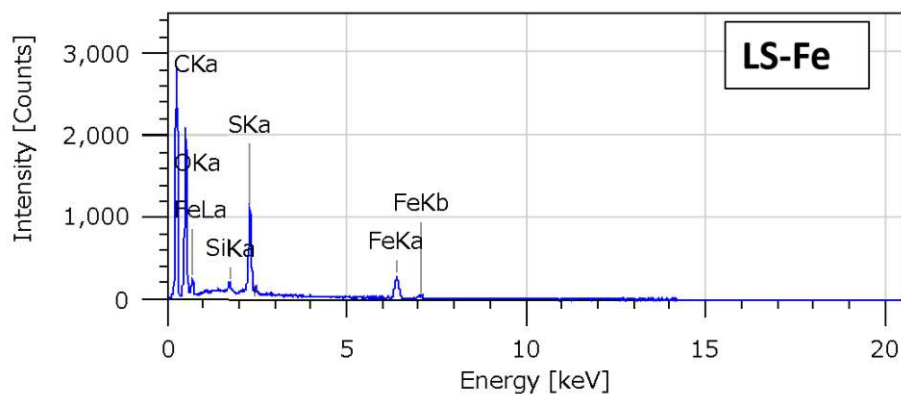


Figure 33: EDS analysis of the LS-Fe capsules

The EDS-results verify all previous results of the successful formation of MPN complexes. The estimated content of carbon, hydrogen, iron, and sulfur are not given, as the results are inaccurate and may lead to wrong conclusions.

AFM images of dry TA-Fe, CaAc-Fe and LS-Fe capsules on glass slides were measured. At first a polynomial surface correction with a polynomial degree of 1 was performed, to correct the tilted surface in the picture. To remove the lines in the picture a histogram line fit was performed. The corrected images of the capsules can be seen in Figure 34. Since the capsules were measured in a dry state, they were in a collapsed state and showed folds and creases. A line profile was measured for a section of each picture, where the capsules did not seem to overlap and if possible, no folds and creases were present. These line profiles were used to calculate the thickness of the capsules. For the calculation the average of the height values of the line profiles at chosen offsets, where no overlapping or folds seemed to be present, was assumed as the capsule thickness. The single-layer thickness was estimated to be half the capsule thickness.

For the line profile of the TA-Fe capsule depicted in Figure 34a, the height from an offset of $0.96 \mu\text{m}$ to $2.12 \mu\text{m}$ was used to calculate the thickness of the capsule. The thickness of the capsule is $11.6 \text{ nm} \pm 4.1 \text{ nm}$ and hence the single-layer thickness can be expected to be $5.8 \text{ nm} \pm 2.1 \text{ nm}$. For the line profile of the CaAc-Fe capsule in Figure 34b the height from an offset of $0.37 \mu\text{m}$ to $2.6 \mu\text{m}$ was used to calculate the thickness of the capsule. The thickness of the capsule is $21.4 \pm 6.0 \text{ nm}$ and hence the single-layer thickness is expected to be $10.7 \text{ nm} \pm 3.0 \text{ nm}$ accordingly. For the line profile of the LS-Fe capsule in Figure 34c the height from an offset of $0.0 \mu\text{m}$ to $1.29 \mu\text{m}$ was used to calculate the thickness of the capsule. The thickness of the capsule is $22.7 \text{ nm} \pm 3.2 \text{ nm}$ and hence the single-layer thickness can be expected to be $11.3 \text{ nm} \pm 1.6 \text{ nm}$.

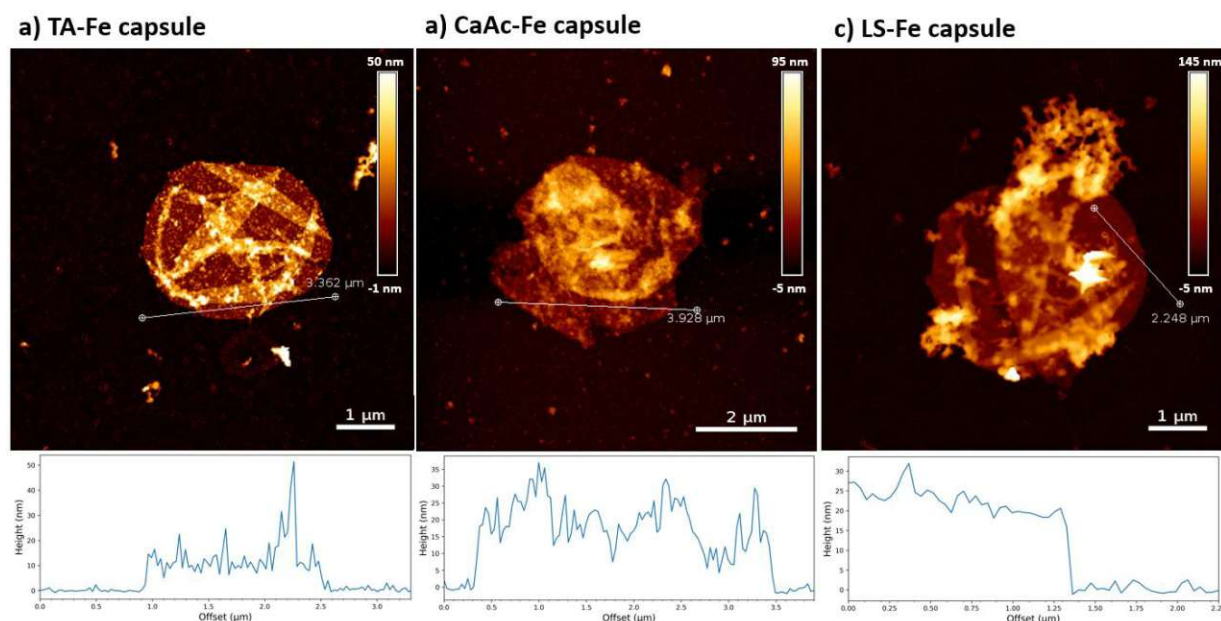


Figure 34: AFM image of a) an TA-Fe capsule b) 2 overlapping CaAc-Fe capsules and c) an LS-Fe capsule. The position of the Line profile below is marked in the image. The color bars show the height of the image (topography).

For a concentration of 0.4 g/l TA and 0.12 g/l Fe which is close to the conditions used in this thesis (0.48 g/l TA and 0.12 g/l Fe) a film thickness of ~ 10.7 nm was reported [5]. This difference in film thickness might be caused by the slightly different procedure, as no MOPS-buffer was added for the capsule formation in this thesis.

3.4 Contact angle

The results for the wettability between the washed and not pre-washed glass slides varied greatly (Figure 35). The unwashed glass slides had a water contact angle of $60 \pm 2^\circ$. This high contact angle may be caused by grease or dust attached to the surface. The pre-washing step of the glass resulted in a much higher wettability with a water contact angle of the glass slide of $26 \pm 7^\circ$. It was visible that a green layer was formed on the glass slide coated with CaAc-Fe while for the other coated glass slides no color change was visible.

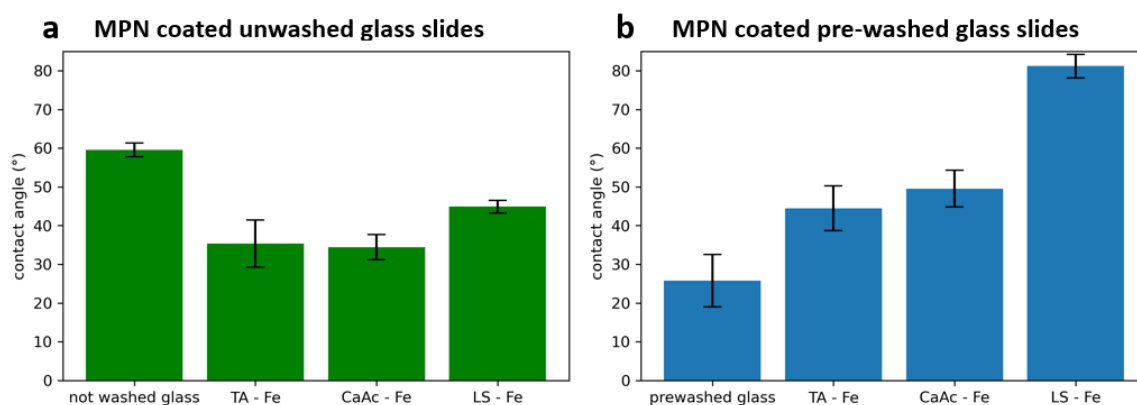


Figure 35: Contact angles of the MPN coated glass slides that were a) not prewashed before coating or b) prewashed by sonicating in water and ethanol

For the coating of not pre-washed glass slides, the MPN coatings resulted in a decrease of the contact angle. In contrast to that, using pre-washed glass slides, the MPN coating increased the contact angle. Different contact angles were found for the MPN coatings, depending on whether the glass was prewashed or not. The TA-Fe and CaAc-Fe coating had roughly the same contact angle. The contact angle of the LS-Fe coating was significantly higher. The highest contact angle was achieved using a washed glass slide and LS-Fe coating and the angle rose to $81 \pm 3^\circ$. Figure 36 depicts some of the pictures for the prewashed glass slide experiments, taken of the water droplets on the glass slides using the contact angle goniometer.

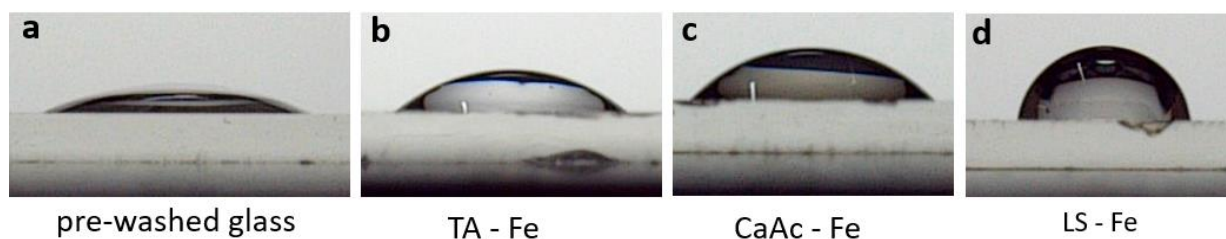


Figure 36: Examples of the images of the drops on the pre-washed glass slides taken with the contact angle goniometer. a) washed glass slide, b) TA-Fe coated glass, c) CaAc-Fe coated glass, d) LS-Fe coated glass

Literature sources using the same washing method for a quartz glass report a slightly higher contact angle of 35° [34]. The contact angle of a glass surface can be influenced by different factors, including the type of cleaning, the chemical structure of the glass and the air humidity [41]. One of the reasons for the lower wettability of the LS-Fe coating might be the higher surface roughness. Since the LS-Fe capsules had a much rougher surface than the TA-Fe or CaAc-Fe capsules it can be concluded that this will be the same for coated glass slides. The TA-Fe wettability was much lower than the one stated by Yun et. al [24]. In the paper contact angles of $7-21^\circ$ were measured. However, the type of glass slides and the coating procedure used is slightly different as the coating solution was premixed and filtrated before immersing

the glass slide. Only one layer was added, but the immersion time was very high (89 h) and after the coating the glass slides were immersed in MOPS buffer.

3.5 Hair dyeing

The dyeing of the pre-bleached hair was successful (Figure 37). For the hair dyed with TA-Fe a purple blue color was achieved. The intensity of the color was not even, and some parts were more intensely dyed than others. The hair dyed with CaAc-Fe was emerald-green and more evenly dyed. For the hair dyed with LS-Fe only a slight color difference was observed. The color of the hair turned straw yellow. This may be because the color of the bleached hair and the LS-Fe coating are very similar to begin with.



Figure 37: Dyed hair samples. a) TA-Fe, b) CaAc-Fe and c) LS-Fe dyed hair. In each picture the left hair strand is undyed, the middle one is dyed once and the right one was dyed 3 times.

It was tried to dye unbleached hair as well, using the CaAc-Fe complexes, but almost no color change could be observed (see Figure 38). The tone of the hair changed a bit to a slightly grayish tone.



Figure 38: Dyed hair sample with unbleached hair dyed with caffeic acid -Fe. The left strand is undyed, the middle strand was dyed once and the right one was dyed 3 times

One possible problem of the dyeing process was that the hair was bound together, which resulted in problems distributing the dyeing solution.

Another approach of dyeing hair using a mixture of tannic acid and gallic acid and in-situ oxidation of Fe^{2+} to Fe^{3+} through oxidation by O_2 was reported in literature [42]. Maybe by in-situ oxidation of iron more stable and even hair dyeing results could be achieved. Another approach that might lead to better results is to premix phenols and iron, adjust the pH and filter the solution before applying it on the hair [34].

3.6 FTIR-spectra

The IR-spectrum of CA is shown in Figure 39. The band at 3459 and 3222 cm^{-1} can be assigned to OH stretching vibrations. The absorption bands between 3030 and 2840 cm^{-1} are caused by C-H stretching vibrations. The absorbance bands found in the fingerprint-region were compared to an IR-spectrum obtained from a spectra-database (spectrabase.com). Both spectra had the same absorption bands, verifying the identity of the CA and the successful measurement of the spectrum.

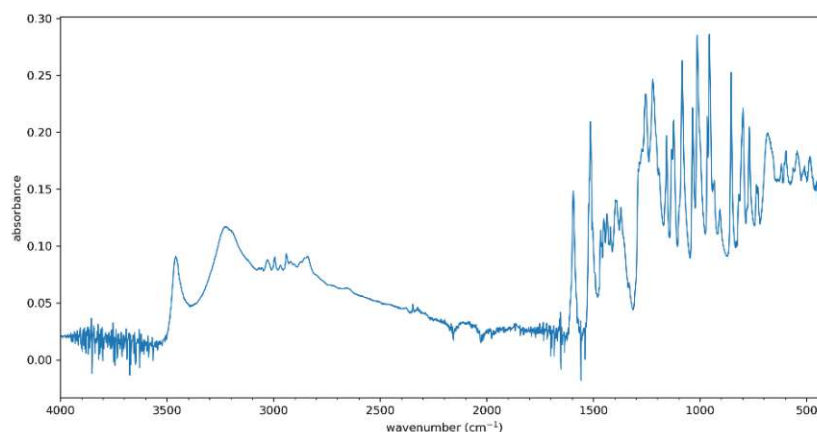


Figure 39: IR-spectrum of coniferyl alcohol

The IR-spectrum of SA is shown in Figure 40. The spectrum was compared with a spectrum of SA of a spectra database (spectrabase.com) and it was found to be the same substance. There was some difference in the absorption between 3600 to 3100 cm^{-1} . While the measured spectrum has a sharp band at 3500 cm^{-1} and a broad band at 3150 cm^{-1} , only one broad band at 3400 cm^{-1} could be found in the spectrum in the database. This broad band could be caused by impurities or humidity present in the SA. The bands at 3400 and 3150 cm^{-1} can be assigned to OH stretching vibrations. The sharp bands at 3000 to 2900 cm^{-1} are caused by C–H stretching vibrations.

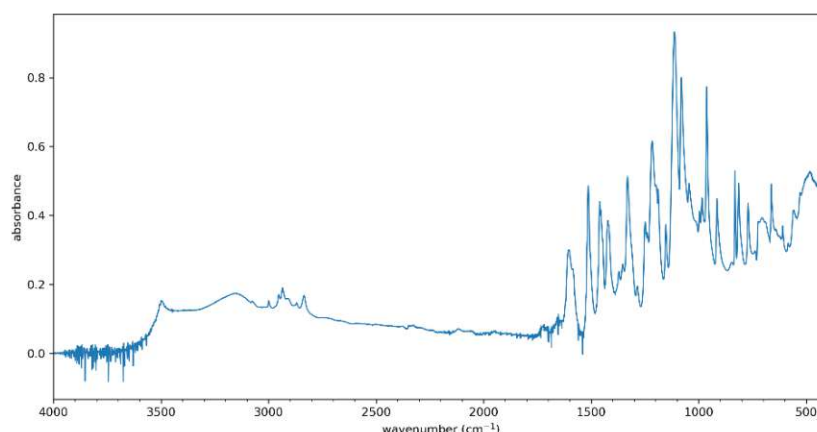


Figure 40: IR-spectrum of sinapyl alcohol

The spectrum of pCA is depicted in Figure 41. No spectrum for comparison could be found in literature. The broad bands at 3442 and 3267 cm^{-1} are caused by OH–stretching vibrations. The smaller sharp bands at 3013, 2936 and 2874 cm^{-1} can be assigned to C–H stretching vibrations.

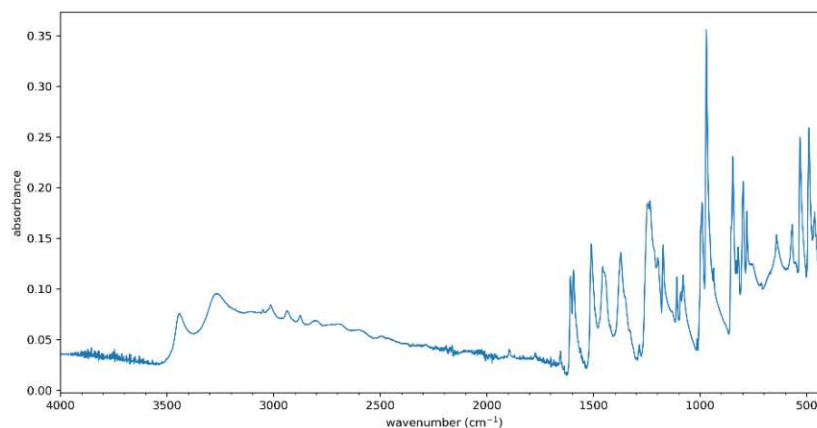


Figure 41: IR-spectrum of para-coumaryl alcohol

The FTIR spectra of the MPN precipitates were obtained by mixing the Phenol and Fe^{3+} solutions and washing and harvesting the formed precipitate. It is assumed that this precipitate has roughly the same chemical structure as the MPN layer formed on different surfaces.

The spectrum of TA and TA-Fe are very similar (see Figure 42). The TA spectrum is in good accordance with spectra found in the literature, but a few band positions are slightly shifted [43,44]. TA has an intense absorption band at 3260 cm^{-1} which is caused by the vibrations of the hydroxyl groups. This broad band is shifted to $\sim 3160\text{ cm}^{-1}$ in the spectrum of TA-Fe. Both the TA and the TA-Fe spectra have C=O stretching vibrations around 1700 cm^{-1} . The band at 1173 cm^{-1} can be assigned to C–O stretching vibrations. The bands at 1081 cm^{-1} , 1173 cm^{-1} and 1307 cm^{-1} in the spectrum of TA are slightly shifted to 1067 cm^{-1} , 1182 cm^{-1} and 1316 cm^{-1} in the spectrum of TA-Fe. The band at 647 cm^{-1} in the spectrum of TA is not visible in the spectrum of TA-Fe.

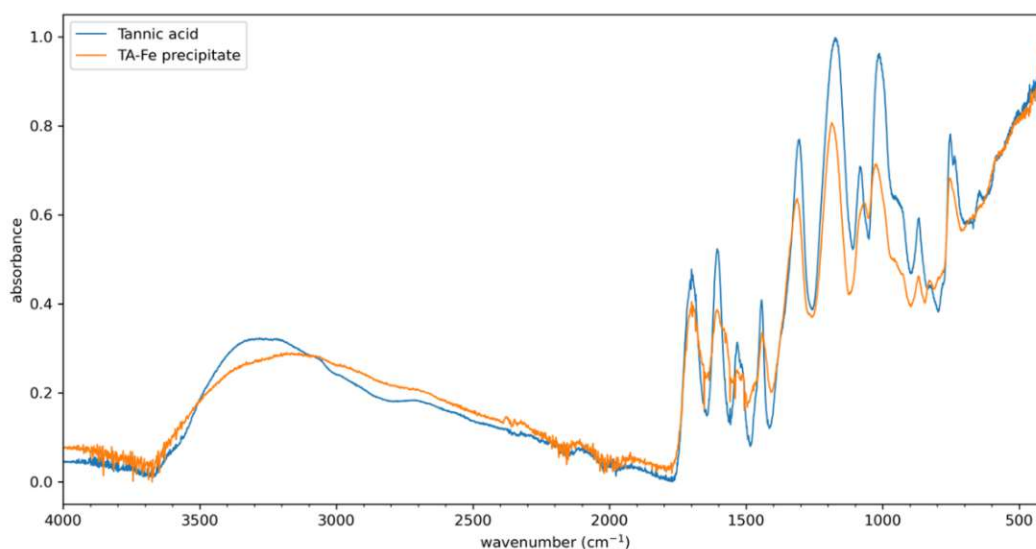


Figure 42: FTIR spectra of tannic acid and TA-Fe precipitate. Both spectra were normalized to enhance comparability.

The FTIR-spectrum of CaAc and CaAc-Fe differ significantly (Figure 43). CaAc has intense bands at 3398 cm^{-1} and 3216 cm^{-1} which can be assigned to OH stretching vibrations. The intense band at 1640 cm^{-1} is caused by C=O stretching vibrations. The bands at 1617 cm^{-1} , 1524 cm^{-1} and 1446 cm^{-1} could be caused by olefinic and aromatic stretching vibrations. The bands at 1272 and 1213 cm^{-1} may be assigned to in-plane bending modes of the olefinic and aromatic C–H bonds. The bands at 814 cm^{-1} and 644 cm^{-1} could be caused by the in-plane bending of the carbonyl group [45,46].

In accordance with literature some of the peaks present in the spectrum of CaAc are not visible in the spectrum of CaAc-Fe [47]. Instead of 2 separate small bands at 3216 cm^{-1} and 3398 cm^{-1} one broad intense band is visible in the spectrum of CaAc-Fe. The spectrum of CaAc-Fe has intense bands at 1610 cm^{-1} , 1262 cm^{-1} and 1185 cm^{-1} as well as a few smaller bands.

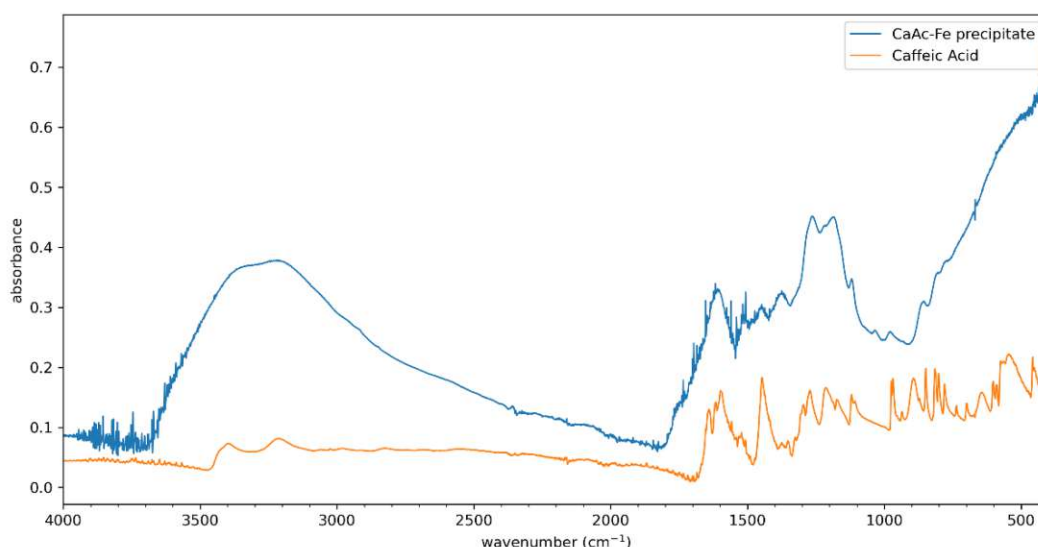


Figure 43: FTIR spectra of CaAc and CaAc-Fe precipitate.

The LS spectrum has a variety of bands (Figure 44). The broad band at 3311 cm^{-1} can be assigned to OH stretching vibrations. The smaller bands at 2940 cm^{-1} are caused by C–H vibrations. A weak band at 1770 cm^{-1} , which may originate from aromatic acetoxy groups, and which was reported for some LS in literature, could not be found. Bands at 1592 cm^{-1} , 1508 cm^{-1} and 1419 cm^{-1} are most likely caused by aromatic skeleton vibrations. The band at 1457 cm^{-1} is caused by a combination of C–H deformation and aromatic ring vibration. These aromatic vibrations should be present in all lignins. The band at 1129 cm^{-1} can be accounted for C–H in plane deformations. Multiple bands are expected at 1260 cm^{-1} and at $1230\text{--}1215\text{ cm}^{-1}$, but the resolution of the used spectrometer was probably not good enough to resolve them and hence they are overlapping. The band at 1034 cm^{-1} is a complex vibration caused by different vibration modes. The sulfonic group vibration can be seen at 616 cm^{-1} [48,49].

The positions of the bands in the spectra of LS and LS-Fe above 1400 cm^{-1} are the same, but the band at 1595 cm^{-1} is much broader in LS-Fe (see Figure 44). The bands below 900 cm^{-1} are much smaller or not apparent in LS-Fe and the absorption is very high in that region for LS-Fe compared to LS. The band at 616 cm^{-1} is shifted to 646 cm^{-1} . This may be caused by bonding between the sulfonate groups and the Fe^{3+} . In the region from 1050 to 1300 cm^{-1} more bands can be distinguished for LS-Fe. The broadening of the band at 1595 cm^{-1} as well as the strong absorption below 1000 cm^{-1} may be caused by residual water.

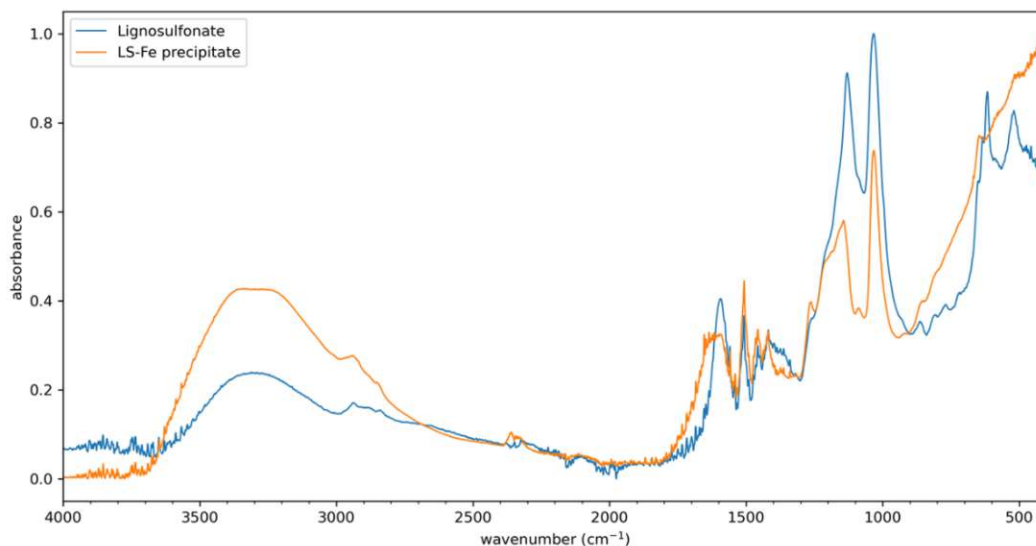


Figure 44: FTIR spectra of lignosulfonate and LS-Fe precipitate. Both spectra were normalized to enhance comparability.

The broad and intense absorption band at $\sim 3300\text{ cm}^{-1}$ was present in the spectra of each of the MPNs measured as well as in FTIR spectra of MPNs found in literature and can be assigned to C–OH stretching modes or water bound to the MPNs [50–52]. The high absorption at wavelengths below 800 cm^{-1} may either be caused by Fe–O stretching vibrations or by water still attached to the MPNs.

4 Summary

In this thesis new phenol-components for the formation of metal phenolic networks (MPNs) were examined and compared to the well-researched tannic acid (TA) – Fe³⁺ MPNs as reference. MPNs can be used to coat a multitude of surfaces and have many potential applications, for example for drug delivery or as hair dye [34,53]. All examined phenols are related to lignin. Caffeic acid (CaAc) is a precursor for the biosynthesis of sinapyl and coniferyl alcohol. Sinapyl alcohol (SA), coniferyl alcohol (CA) and paracoumaryl alcohol (pCA) are referred to as monolignols and are the main building blocks of lignin. Lignosulfonate (LS) is formed from lignin in the sulfite process and is an abundant by-product. Using different phenols for MPN formation, different characteristics can be achieved, and thus new fields of usage may be opened.

First, whether MPNs can be formed from the new phenols or not should be verified using a quartz crystal microbalance (QCM). Multiple layers of MPNs were coated on the QCM crystal and the mass-change after each step was measured. Two different approaches were examined. One approach was to mix all chemicals (phenol and Fe³⁺ solution and MOPS buffer) together for coating, the other approach was dipping the QCM crystal into Fe³⁺ and phenol solution consecutively. The mixing approach proved to be faulty, due to precipitation of Fe³⁺ on the crystal and did not yield useful results. The approach using consecutive dipping yielded more stable results and suggested that MPN formation using pCA could be possible. Because SA and CA demonstrated neither considerable mass gain nor color change due to complex formation no further experiments were performed with those 2 phenols. The measurements were unstable altogether and had poor repeatability.

Therefore UV-Vis spectroscopy was used to monitor layer growth. The phenol to metal ratio was optimized for pCA, CaAc and LS. The phenol and metal solutions were mixed in different ratios and the UV-Vis absorption of the mixtures was monitored. The optimal molar ratio for pCA-Fe and CaAc-Fe respectively was 1:1 and 1:2. For LS-Fe a mass ratio of 1:1, phenol to FeCl₃·6H₂O was found to be the most effective. This mass ratio roughly equals a mass ratio of 5:1 phenol to Fe³⁺. The influence of the pH on the color of the CaAc-Fe complex and the layer formation ability was examined by at first mixing CaAc and Fe-solutions and then adjusting the pH in a range from 1 to 11. At low pH the complex is almost colorless with a slight yellow tone and then turns green at increasing pH. At a pH above 7 it turns black and then red brown

at pH 9 and above. The ability of CaAc and LS to form complexes with other metal ions (Mn^{2+} , Al^{3+} , Cu^{2+} , Zr^{4+} and Co^{2+} ,) was examined and Zr^{4+} exhibited promising results.

The cuvettes were coated with multiple layers of MPN. For coating the phenol and metal solutions were mixed with some additional water. All coatings absorbed at wavelengths below 350 nm. LMCT absorption bands were found for cuvettes coated with TA-Fe and CaAc-Fe layers at 570 and 650 nm respectively. The CaAc-Zr coated cuvette had an intense absorption band at 350 nm. The formation of pCA-Fe and LS-Zr coated cuvettes failed. After adapting the coating process using consecutive dipping like in the QCM experiments a slight absorption of the pCA-Fe layer could be reached, and a few blue spots were visible on the cuvette walls. However, the expected charge transfer band at 600 nm was not visible. The TA-Fe, LS-Fe and CaAc-Fe cuvettes were coated using different concentrations of reagents to determine the concentration dependence of the layer formation. The stepwise layer growth was, according to the gain of absorption, linear. A change in the concentration of the reagents resulted in a strong change of layer intensity for TA-Fe in the examined concentration range. For CaAc-Fe the concentration of reactants and the intensity of the formed layer correlated directly. For LS-Fe only a weak influence of concentration could be found. The stability of the TA-Fe, CaAc-Fe and LS-Fe layers at different conditions was examined by filling the coated cuvettes with different disassembly solutions (pH 1, pH 4, EDTA at pH 4.8, sodium ascorbate at pH 7.3, MOPS buffer at pH 7.4. and pH 11). Before the measurements the solutions were exchanged to remove dissolved MPN components. The layers were rapidly disassembled at pH 1, pH 11 and in EDTA solution. Part of the absorption at low wavelength remained at pH 1 for CaAc-Fe but the LMCT band disappeared completely. At pH 4 the TA-Fe and CaAc-Fe layers degraded slowly. The LS-Fe layers degraded the slowest, even after 68 h, 87 % of the absorption remained. The TA-Fe and CaAc-layer are stable at pH 7.4 but the LS-Fe layer degrades slowly. A change in the absorption spectrum was noticed for the TA-Fe layer at neutral pH and the color of the coating turned from blue to purple. The degradation behavior differed the most in the sodium ascorbate solution. LS-Fe degraded medium fast with the same behavior as the other degradations (fast in the beginning, then slows down). For CaAc-Fe it took roughly 2 hours till the degradation started and the degradation of the TA-Fe layer began after ~40 hours.

After characterization of the layer disassembly and assembly conditions, the formation of free-standing capsules was attempted. To form the capsules PS microspheres were coated by mixing them with phenol and metal solution. The excess reagents were removed by washing with water. A centrifuge was used to settle down the particles and the supernatant solution was removed.

After washing, the PS-spheres were dissolved by adding THF. The free-standing capsules were subsequently redispersed in water. Pictures of the capsules were obtained using an optical microscope, SEM, TEM, and AFM. The single layer thickness for the capsules was $5.8 \text{ nm} \pm 2.1 \text{ nm}$, $11.3 \text{ nm} \pm 1.6 \text{ nm}$ and $10.7 \text{ nm} \pm 3.0 \text{ nm}$ for TA-Fe, CaAc-Fe and LS-Fe capsules respectively. Smooth and stable capsules were received using TA-Fe and CaAc-Fe coatings. The LS-Fe capsules were brittle, and a lot of complex debris was attached to them. The EDS spectra of the capsules verified the presence of carbon and Fe and sulfur for the LS-Fe capsules as expected. The formation of pCA-Fe, LS-Zr and CaAc-Zr capsules failed.

To determine the wettability of the MPNs washed and not prewashed glass slides were coated with MPNs, and the contact angle of a water drop dropped on the slides was measured. TA-Fe and CaAc-Fe both had similar high wettability. The wettability of LS-Fe coated glass slides was significantly lower.

Bleached human hair was dyed using TA-Fe, CaAc-Fe and LS-Fe and resulted in blue, emerald-green, and straw-yellow color respectively.

The major results are summed up in Table 11.

4 Summary

Table 11: Summary of most important results of this thesis for Phenol-Iron(III) MPN experiments. ○ Successful experiment/formation, △ partial successful or only successful with limitations, × not successful, - not examined. *blue color was only slightly visible

Phenol used for MPN assembly	Tannic acid	Para coumaryl alcohol	Coniferyl alcohol	Sinapyl alcohol	Ligno-sulfonate	Caffeic Acid
mass gain QCM dipping ratio optimized	○	○	×	×	×	-
LMCT band wavelength [nm]	-	○	-	-	○	○
color of complex	570	600	×	×	×	650
layer formation in cuvette	blue	blue*	-	-	straw-yellow	green
concentration dependence layer formation	○	△	-	-	○	○
disassembly conditions:	strong	-	-	-	weak	linear
pH 1	fast	-	-	-	fast	fast
pH 4	slow	-	-	-	very slow	slow
EDTA	fast	-	-	-	fast	fast
sodium ascorbate	slow	-	-	-	medium fast	slow
pH 7.4	stable	-	-	-	slow	stable
pH 12	fast	-	-	-	fast	fast
capsule formation	○	×	-	-	△	○
single layer thickness capsule	6 ± 2 nm	-	-	-	11 ± 2 nm	11 ± 3 nm
wettability	high	-	-	-	medium	high
color as hair dye	blue	-	-	-	straw-yellow	emerald-green

5 Conclusion

In this thesis never before used phenolic compounds (pCA, CA, SA, CaAc and LS) were utilized for the formation of metal phenolic networks. Fe^{3+} was chosen as main metal-ion for MPN formation and TA was used as reference phenolic compound, as it is already extensively researched.

The formation of MPN using CaAc and LS was successful. No positive signs for MPN formation could be verified for SA and CA. For pCA it seemed that some interaction with Fe^{3+} does take place, mass gain using QCM was observed and a weak LMCT band is present. However no continuous MPN coating was achieved and therefore no capsules could be formed. The CaAc-Fe and LS-Fe MPNs were further characterized and compared with the TA-Fe MPN. Each of the MPNs exhibited a different color. Changing the concentrations of the phenol and Fe^{3+} solutions revealed the different concentration dependence of the MPN layer formation for each of the MPNs. The disassembly conditions for the MPNs varied slightly. The capsule thickness and stability were different as well. CaAc-Fe and TA-Fe coatings formed stable and smooth capsules. The LS-Fe capsules were brittle and uneven with precipitate attached to them. CaAc-Fe and TA-Fe coatings exhibited high wettability compared to the LS-Fe coating. The new CaAc-Fe and LS-Fe coatings were used to dye hair and resulted in emerald-green and straw-yellow color respectively.

The toolbox of usable phenols for MPN formation was expanded in this thesis and the new MPNs could be used for different future applications e.g., as hair dye, adjustment of the wettability of surfaces, antimicrobial coating, encapsulation of microorganisms or drugs.

6 Outlook

In this thesis different phenolic compounds (TA, LS and CaAc) were successfully used for the assembly of MPNs and could be used for the coating of various substrates including glass, PS and PMMA.

Further experiments to characterize the new materials should be conducted. Raman spectroscopy could be used to get more information about the chemical structure of the MPNs. Furthermore, no experiments revealing the actual phenol to metal ratio in the MPNs have been conducted till now. The possibility to use different metal ions and hence adapt the traits of the MPNs would be of interest as well as only a quick look at the possibility of using Zr^{4+} for MPN formation was taken.

Different uses for the MPNs could be researched. The potential as hair dye could already be demonstrated, however the process still needs optimization. The encapsulating traits of the new MPNs could be used to coat bacteria and viruses to protect them and temporarily stop proliferation. By changing the conditions, they could then be disassembled when necessary. LS exhibits antimicrobial activity and is not toxic which is why LS-Fe coatings may be usable for antimicrobial coatings, to for example increase the shelf life of fruits [54,55]. The double bond in the side chain of CaAc as well as the carboxy group may be used to add further functionalization for different uses of CaAc based MPNs. CaAc has antioxidant, antimicrobial, antiviral and anticarcinogenic effects [56–58]. Through esterification caffeic acid phenyl ester (CAPE) can be formed, which has cytotoxic effects on tumor cell lines [59]. Malignant tumor have an acidic microenvironment, which could be used to disassemble MPNs at the tumor site specifically [60].

List of Abbreviations

AFM	Atomic Force Microscopy
CA	Coniferyl Alcohol
CaAc	Caffeic Acid
EDS	Energy Dispersive X-Ray Spectroscopy
EDTA	Disodium dihydrogen ethylenediaminetetraacetic acid
LMCT	Ligand-to-Metal Charge Transfer
LS	Lignosulfonate
MOPS	3-(N-morpholino)propanesulfonic acid
MPN	Metal Phenolic Network
pCA	para-Coumarylalcohol
PMMA	Poly(methyl methacrylate)
QCM	Quartz Crystal Microbalance
SA	Sinapyl Alcohol
SEM	Scanning Electron Microscope
TA	Tannic Acid
TEM	Transmission Electron Microscope
THF	Tetrahydrofuran

7 References

1. Park JH, Kim K, Lee J, Choi JY, Hong D, Yang SH, u. a. Frontispiece: A Cytoprotective and Degradable Metal-Polyphenol Nanoshell for Single-Cell Encapsulation. *Angew Chem Int Ed.* 10. November 2014;53(46):n/a-n/a.
2. Rahim MdA, Lin G, Tomanin PP, Ju Y, Barlow A, Björnmalm M, u. a. Self-Assembly of a Metal–Phenolic Sorbent for Broad-Spectrum Metal Sequestration. *ACS Appl Mater Interfaces.* 22. Januar 2020;12(3):3746–54.
3. Han SY, Kang EK, Choi IS. Iron Gall Ink Revisited: A Surfactant-Free Emulsion Technology for Black Hair-Dyeing Formulation. *Cosmetics.* März 2021;8(1):9.
4. Guo J, Ping Y, Ejima H, Alt K, Meissner M, Richardson JJ, u. a. Engineering Multifunctional Capsules through the Assembly of Metal–Phenolic Networks. *Angew Chem Int Ed.* 2014;53(22):5546–51.
5. Ejima H, Richardson JJ, Liang K, Best JP, Van Koeverden MP, Such GK, u. a. One-Step Assembly of Coordination Complexes for Versatile Film and Particle Engineering. *Science.* 12. Juli 2013;341(6142):154–7.
6. Zhong QZ, Pan S, Rahim MdA, Yun G, Li J, Ju Y, u. a. Spray Assembly of Metal–Phenolic Networks: Formation, Growth, and Applications. *ACS Appl Mater Interfaces.* 3. Oktober 2018;10(39):33721–9.
7. Strasburger E, Sitte P, Herausgeber. *Lehrbuch der Botanik für Hochschulen.* 35. Aufl. Heidelberg Berlin: Spektrum, Akad. Verl; 2002. 1123 S. (Spektrum-Lehrbuch).
8. Vanholme R, Demedts B, Morreel K, Ralph J, Boerjan W. Lignin Biosynthesis and Structure. *Plant Physiol.* 1. Juli 2010;153(3):895–905.
9. Yadav V, Wang Z, Wei C, Amo A, Ahmed B, Yang X, u. a. Phenylpropanoid Pathway Engineering: An Emerging Approach towards Plant Defense. *Pathogens.* 23. April 2020;9(4):312.
10. Atta-ur-Rahman, Herausgeber. *Bioactive natural products.* Amsterdam Oxford Cambridge, MA Elsevier; 2022. 488 S. (Studies in natural products chemistry).
11. Schomburg D, Michal G, Herausgeber. *Biochemical pathways: an atlas of biochemistry and molecular biology.* 2nd ed. Hoboken, N.J: John Wiley & Sons; 2012. 398 S.
12. Bartzoka ED, Lange H, Thiel K, Crestini C. Coordination Complexes and One-Step Assembly of Lignin for Versatile Nanocapsule Engineering. *ACS Sustain Chem Eng.* 3. Oktober 2016;4(10):5194–203.
13. Behr A, Seidensticker T. *Einführung in die Chemie nachwachsender Rohstoffe: Vorkommen, Konversion, Verwendung.* Berlin [Heidelberg]: Springer Spektrum; 2018. 392 S. (Lehrbuch).
14. Huang J. *Materials from modified lignin.* 1st edition. Cambridge, MA: Elsevier; 2019.

15. Khabarov YuG, Veshnyakov VA, Shergin AE. Electrochemical synthesis and biological activity of iron lignosulfonate. *Russ Chem Bull.* Mai 2019;68(5):1081–7.
16. Sodium Ligninsulfonate 8061-51-6 | Tokyo Chemical Industry Co., Ltd.(APAC) [Internet]. [zitiert 4. Oktober 2023]. Verfügbar unter: <https://www.tcichemicals.com/SG/en/p/L0098>
17. Lange H, Schiffels P, Sette M, Sevastyanova O, Crestini C. Fractional Precipitation of Wheat Straw Organosolv Lignin: Macroscopic Properties and Structural Insights. *ACS Sustain Chem Eng.* 3. Oktober 2016;4(10):5136–51.
18. Harrington MJ, Masic A, Holten-Andersen N, Waite JH, Fratzl P. Iron-Clad Fibers: A Metal-Based Biological Strategy for Hard Flexible Coatings. *Science.* 9. April 2010;328(5975):216–20.
19. Beecher GR. Overview of Dietary Flavonoids: Nomenclature, Occurrence and Intake. *J Nutr.* Oktober 2003;133(10):3248S-3254S.
20. Rahim MdA, Kempe K, Müllner M, Ejima H, Ju Y, van Koeverden MP, u. a. Surface-Confining Amorphous Films from Metal-Coordinated Simple Phenolic Ligands. *Chem Mater.* 25. August 2015;27(16):5825–32.
21. Tannic acid [Internet]. American Chemical Society. [zitiert 19. September 2023]. Verfügbar unter: <https://www.acs.org/molecule-of-the-week/archive/t/tannic-acid.html>
22. Mejbaum-Katzenellenbogen null, Kudrewicz-Hubicka Z. Application of urea, ferric ammonium sulphate and casein for determination of tanning substances in plants. *Acta Biochim Pol.* 1966;13(1):57–67.
23. Rahim MdA, Ejima H, Cho KL, Kempe K, Müllner M, Best JP, u. a. Coordination-Driven Multistep Assembly of Metal–Polyphenol Films and Capsules. *Chem Mater.* 25. Februar 2014;26(4):1645–53.
24. Yun G, Besford QA, Johnston ST, Richardson JJ, Pan S, Biviano M, u. a. Self-Assembly of Nano- to Macroscopic Metal–Phenolic Materials. *Chem Mater.* 28. August 2018;30(16):5750–8.
25. Sauerbrey G. Verwendung von Schwingquarzen zur Wägung dünner Schichten und zur Mikrowägung. *Z Für Phys.* April 1959;155(2):206–22.
26. Matissek R, Steiner G, Fischer M. *Lebensmittelanalytik.* 4. Aufl. Berlin Heidelberg: Springer; 2009. 496 S.
27. Agilent Technologies, Inc. *The Basics of UV-Vis Spectrophotometry* [Internet]. 2021. Verfügbar unter: <https://www.agilent.com/cs/library/primers/public/primer-uv-vis-basics-5980-1397en-agilent.pdf>
28. Stuart BH. *Infrared Spectroscopy: Fundamentals and Applications* [Internet]. 1. Aufl. Wiley; 2004 [zitiert 9. August 2023]. (Analytical Techniques in the Sciences). Verfügbar unter: <https://onlinelibrary.wiley.com/doi/book/10.1002/0470011149>

29. What is Microscopy? [Internet]. The University of Edinburgh. 2018 [zitiert 26. Mai 2023]. Verfügbar unter: <https://www.ed.ac.uk/clinical-sciences/edinburgh-imaging/for-patients-study-participants/tell-me-more-about-my-scan/what-is-microscopy>
30. Watt IM. The Principles and Practice of Electron Microscopy [Internet]. 2. Aufl. Cambridge: Cambridge University Press; 1997 [zitiert 26. Mai 2023]. Verfügbar unter: <https://www.cambridge.org/core/books/principles-and-practice-of-electron-microscopy/C6204DC9D7E7FA9C1594C62BA1E813B6>
31. Haugstad G. Atomic Force Microscopy: Understanding Basic Modes and Advanced Applications [Internet]. Hoboken, NJ, USA: John Wiley & Sons, Inc.; 2012 [zitiert 21. Juli 2023]. Verfügbar unter: <http://doi.wiley.com/10.1002/9781118360668>
32. Encyclopedia of nanotechnology. New York: Springer; 2012.
33. Mota FL, Queimada AJ, Pinho SP, Macedo EA. Aqueous Solubility of Some Natural Phenolic Compounds. *Ind Eng Chem Res.* 1. August 2008;47(15):5182–9.
34. Geng H, Zhuang L, Li M, Liu H, Caruso F, Hao J, u. a. Interfacial Assembly of Metal–Phenolic Networks for Hair Dyeing. *ACS Appl Mater Interfaces.* 16. Juni 2020;acsami.0c06928.
35. Monhemius J. Precipitation diagrams for metal hydroxides, sulphides, arsenates and phosphates. *Trans Inst Min Metall.* 1. Dezember 1977;86:C202–6.
36. Carrasco J, Kovács K, Czech V, Fodor F, Lucena JJ, Vértés A, u. a. Influence of pH, Iron Source, and Fe/Ligand Ratio on Iron Speciation in Lignosulfonate Complexes Studied Using Mössbauer Spectroscopy. Implications on Their Fertilizer Properties. *J Agric Food Chem.* 4. April 2012;60(13):3331–40.
37. Xu H, Nishida J, Ma W, Wu H, Kobayashi M, Otsuka H, u. a. Competition between Oxidation and Coordination in Cross-Linking of Polystyrene Copolymer Containing Catechol Groups. *ACS Macro Lett.* 17. April 2012;1(4):457–60.
38. Friedman M, Jürgens HS. Effect of pH on the Stability of Plant Phenolic Compounds. *J Agric Food Chem.* 1. Juni 2000;48(6):2101–10.
39. Makkar HPS, Becker K. Effect of pH, Temperature, and Time on Inactivation of Tannins and Possible Implications in Detannification Studies. *J Agric Food Chem.* 1. Januar 1996;44(5):1291–5.
40. Lee H, Park J, Han SY, Han S, Youn W, Choi H, u. a. Ascorbic acid-mediated reductive disassembly of Fe³⁺-tannic acid shells in degradable single-cell nanoencapsulation. *Chem Commun.* 2020;56(89):13748–51.
41. Engländer T, Wiegel D, Naji L, Arnold K. Dehydration of Glass Surfaces Studied by Contact Angle Measurements. *J Colloid Interface Sci.* Mai 1996;179(2):635–6.
42. Han S, Hong SP, Kang E, Kim B, Lee H, Kim W, u. a. Iron Gall Ink Revisited: Natural Formulation for Black Hair-Dyeing. *Cosmetics.* 1. April 2019;6(2):23.

43. Wahyono T, Astuti DA, Gede Wiryawan IK, Sugoro I, Jayanegara A. Fourier Transform Mid-Infrared (FTIR) Spectroscopy to Identify Tannin Compounds in The Panicle of Sorghum Mutant Lines. *IOP Conf Ser Mater Sci Eng.* 1. Juni 2019;546(4):042045.
44. Li YM, Miao X, Wei ZG, Cui J, Li SY, Han R, u. a. Iron-tannic acid nanocomplexes: Facile synthesis and application for removal of methylene blue from aqueous solution. 1. Oktober 2016;11:1045–61.
45. Catauro M, Barrino F, Dal Poggetto G, Crescente G, Piccolella S, Pacifico S. New SiO₂/Caffeic Acid Hybrid Materials: Synthesis, Spectroscopic Characterization, and Bioactivity. *Materials.* 15. Januar 2020;13(2):394.
46. Tosovic J. Spectroscopic features of caffeic acid: Theoretical study. *Kragujev J Sci.* 2017;(39):99–108.
47. Singh K, Kumar A. Kinetics of complex formation of Fe(III) with caffeic acid: Experimental and theoretical study. *Spectrochim Acta A Mol Biomol Spectrosc.* März 2019;211:148–53.
48. Boeriu CG, Bravo D, Gosselink RJA, Van Dam JEG. Characterisation of structure-dependent functional properties of lignin with infrared spectroscopy. *Ind Crops Prod.* September 2004;20(2):205–18.
49. Rodríguez-Lucena P, Lucena JJ, Hernández-Apaolaza L. Relationship between the structure of Fe-Lignosulfonate complexes determined by FTIR spectroscopy and their reduction by the leaf Fe reductase. 30. Juni 2009 [zitiert 3. August 2023]; Verfügbar unter: <https://escholarship.org/uc/item/9k69q71d>
50. Huang F, Jiang X, Sallam MA, Zhang X, He W. A Nanocrystal Platform Based on Metal-Phenolic Network Wrapping for Drug Solubilization. *AAPS PharmSciTech.* April 2022;23(3):76.
51. Xu W, Pan S, Noble BB, Chen J, Lin Z, Han Y, u. a. Site-Selective Coordination Assembly of Dynamic Metal-Phenolic Networks. *Angew Chem Int Ed [Internet].* 22. August 2022 [zitiert 20. Juli 2023];61(34). Verfügbar unter: <https://onlinelibrary.wiley.com/doi/10.1002/anie.202208037>
52. Lin Z, Zhou J, Cortez-Jugo C, Han Y, Ma Y, Pan S, u. a. Ordered Mesoporous Metal-Phenolic Network Particles. *J Am Chem Soc.* 8. Januar 2020;142(1):335–41.
53. Ping Y, Guo J, Ejima H, Chen X, Richardson JJ, Sun H, u. a. pH-Responsive Capsules Engineered from Metal-Phenolic Networks for Anticancer Drug Delivery. *Small.* Mai 2015;11(17):2032–6.
54. Chen M, Li Y, Liu H, Zhang D, Shi QS, Zhong XQ, u. a. High value valorization of lignin as environmental benign antimicrobial. *Mater Today Bio.* Februar 2023;18:100520.
55. EFSA Panel on Additives and Products or Substances used in Animal Feed (FEEDAP), Bampidis V, Azimonti G, Bastos M de L, Christensen H, Dusemund B, u. a. Safety of lignosulphonate for all animal species. *EFSA J [Internet].* Februar 2020 [zitiert 21. Juli 2023];18(2). Verfügbar unter: <https://data.europa.eu/doi/10.2903/j.efsa.2020.6000>

56. Zhang Z, Wang D, Qiao S, Wu X, Cao S, Wang L, u. a. Metabolic and microbial signatures in rat hepatocellular carcinoma treated with caffeic acid and chlorogenic acid. *Sci Rep.* 3. Juli 2017;7(1):4508.
57. Genaro-Mattos TC, Mauricio ÂQ, Rettori D, Alonso A, Hermes-Lima M. Correction: Antioxidant Activity of Caffeic Acid against Iron-Induced Free Radical Generation—A Chemical Approach. *PLOS ONE.* 3. November 2015;10(11):e0142402.
58. Langland J, Jacobs B, Wagner CE, Ruiz G, Cahill TM. Antiviral activity of metal chelates of caffeic acid and similar compounds towards herpes simplex, VSV-Ebola pseudotyped and vaccinia viruses. *Antiviral Res.* Dezember 2018;160:143–50.
59. Nagaoka T. Selective antiproliferative activity of caffeic acid phenethyl ester analogues on highly liver-Metastatic murine colon 26-L5 carcinoma cell line. *Bioorg Med Chem.* Oktober 2002;10(10):3351–9.
60. Justus CR, Dong L, Yang LV. Acidic tumor microenvironment and pH-sensing G protein-coupled receptors. *Front Physiol* [Internet]. 2013 [zitiert 2. August 2023];4. Verfügbar unter: <http://journal.frontiersin.org/article/10.3389/fphys.2013.00354/abstract>

8 List of Figures

Figure 1: Chemical structure of the 3 main monolignols paracoumaryl alcohol, coniferyl alcohol and sinapyl alcohol.....	2
Figure 2: Chemical structure of caffeic acid	2
Figure 3: Idealized scheme of sulfonation and hydrolyzation of lignin during sulfite process (Source: Wikimedia)	3
Figure 4: "Generic" structure of lignosulfonates [17].	3
Figure 5: Formation of mono-, bis- and tris-complexes between Fe(III) and Phenols at different pH values.....	4
Figure 6: Chemical structure of tannic acid	5
Figure 7: QCM crystal inserted in sample holder.	11
Figure 8: Illustration of the capsule formation process. The phenol- and Fe ³⁺ solution are added to the vial with the microspheres. Washing takes place by centrifuging and replacing the supernatant solution with water. To dissolve the PS, the MPN-capsules are washed with THF 2 or 3 times, and the capsules are resuspended in water.	18
Figure 9: a) Image of the CaAc-Fe coating process of the glass slide and b) the coated glass slide	19
Figure 10: Total mass gain of QCM-Crystal during MPN coating process. Note: SEM was used for the errorbars instead of STD.....	21
Figure 11: 1 g/l of FeCl ₃ .6H ₂ O dissolved in 10 mmol/l MOPS and water for comparison....	22
Figure 12: Results for the mass gain of the MPN coating process using the dipping method. The upper diagrams (a,b) illustrate the total mass gain for all steps. The lower pictures (c,d) depict the stepwise mass gain. The errorbars were generated using SEM instead of STD to increase readability of the diagrams. a,c) TA-Fe and pCA-Fe, b,d) SA-Fe, CA-Fe and LS-Fe	24
Figure 13: QCM crystal consecutively dipped into paracoumaryl alcohol and iron solution with blue spots on the surface.	25
Figure 14: Disassembly of MPN coatings on QCM crystals at different conditions. The starting mass before the disassembly was between 1026 ng and 1448 ng	25
Figure 15: Caffeic Acid and Iron mixed in different molar ratios. a) directly after mixing, b) after one day	26
Figure 16: Lignosulfonate and FeCl ₃ .6H ₂ O solution mixed in different mass ratios. a) directly after mixing, b) after one day	27

Figure 17: UV-Vis data for optimization of the Phe:Fe ratio. Phenol and Iron-solution were mixed in different ratios and diluted with water. a) Results for CaAc-Fe at 650 nm (absorption maximum of LMCT band), b) results for LS-Fe, note the mass ratio of the lignosulfonate and Iron-salt is depicted, c) results for pCA-Fe at 600 nm (absorption maximum of LMCT band)	28
Figure 18: Image of the CaAc-Fe complex at different pH. a) Image taken right after mixing the components and adjusting the pH, b) Image taken after 3 days	28
Figure 19: Absorption spectra of the (a) Ca-Fe complex solution directly after mixing and b) of the CaAc-Fe layer formed on the cuvette walls after one week	29
Figure 20: a) Image of mixture of CaAc and Fe-solution and precipitate after centrifugation, b) Mixture of LS and Zr-solution and color of the mutual solutions for comparison	30
Figure 21: a) Absorption Spectra of the MPN coated cuvettes and b) images of coated cuvettes demonstrating the color of the coating. In the red circle a blue spot of pCA - Fe MPN is visible but no continuous coating was formed. For the formation of the pCA-Fe layer iron solution and buffered pCA solution were put into the cuvette in succession.	30
Figure 22: Multistep MPN layer build up monitored using UV-Vis. The ratio of phenol to iron was kept constant for all experiments. a) TA-Fe, b) CaAc-Fe c) LS-Fe.....	32
Figure 23: Layer build-up of the CaAc-Zr layer, monitored using UV-Vis spectroscopy.	32
Figure 24: Time dependence of the MPN coating process. a) TA-Fe coating, b) CaAc-Fe coating, c) LS-Fe coating	33
Figure 25: Disassembly of the MPN layers at different conditions, monitored by UV-Vis spectrophotometry. a) disassembly of the TA-Fe layer, b) disassembly of the CaAc-layer, c) disassembly of the LS-Fe layer	33
Figure 26: Change of the UV-Vis absorption spectrum of TA-Fe after 2 h in pH 7.4 MOPS solution	35
Figure 27: Change of the UV-Vis absorption spectrum of CaAc-Fe after 92 h in pH 1 solution	35
Figure 28: Capsule preparation of TA-Fe, CaAc-Fe and LS-Fe capsules (left to right in each picture). a) After addition of the reagent the color of the solution changes, b) excess reagents are removed by washing with water c) the PS-spheres are dissolved in THF, and the capsules remain.....	36
Figure 29: Optical microscope image of LS-Fe capsules. Broken capsules and debris are visible.	38

Figure 30: Optical microscope, TEM, and SEM pictures of a) TA-Fe, b) CaAc-Fe and c) LS-Fe capsules.	38
Figure 31: EDS spectrum of the TA-Fe capsules.....	39
Figure 32: EDS spectrum of the CaAc-Fe capsules.....	39
Figure 33: EDS analysis of the LS-Fe capsules.....	40
Figure 34: AFM image of a) an TA-Fe capsule b) 2 overlapping CaAc-Fe capsules and c) an LS-Fe capsule. The position of the Line profile below is marked in the image. The color bars show the height of the image (topography).....	41
Figure 35: Contact angles of the MPN coated glass slides that were a) not prewashed before coating or b) prewashed by sonicating in water and ethanol.....	42
Figure 36: Examples of the images of the drops on the pre-washed glass slides taken with the contact angle goniometer. a) washed glass slide, b) TA-Fe coated glass, c) CaAc-Fe coated glass, d) LS-Fe coated glass.....	42
Figure 37: Dyed hair samples. a) TA-Fe, b) CaAc-Fe and c) LS-Fe dyed hair. In each picture the left hair strand is undyed, the middle one is dyed once and the right one was dyed 3 times.	43
Figure 38: Dyed hair sample with unbleached hair dyed with caffeic acid -Fe. The left strand is undyed, the middle strand was dyed once and the right one was dyed 3 times.....	44
Figure 39: IR-spectrum of coniferyl alcohol.....	45
Figure 40: IR-spectrum of sinapyl alcohol.....	45
Figure 41: IR-spectrum of para-coumaryl alcohol.....	46
Figure 42: FTIR spectra of tannic acid and TA-Fe precipitate. Both spectra were normalized to enhance comparability.....	47
Figure 43: FTIR spectra of CaAc and CaAc-Fe precipitate.....	48
Figure 44: FTIR spectra of lignosulfonate and LS-Fe precipitate. Both spectra were normalized to enhance comparability.	49
Figure 45: Results of the QCM disassembly experiment for pCA-Fe and LS-Fe coated QCM crystals. A negative mass loss indicates mass gain. The starting mass of the layer was between 729 and 1299 ng.	68
Figure 46: Spectra of iron(III)chloride and all phenols examined in the thesis in aqueous solution.....	68
Figure 47: Spectrum of the paracoumaryl alcohol and iron solution showing the LMCT band.....	69

Figure 48: Disassembly of the MPN layers at different conditions, monitored by UV-Vis spectrophotometry. a) disassembly of the TA-Fe layer, b) disassembly of the CaAc-layer, c) disassembly of the LS-Fe layer 69

9 List of Tables

Table 1: Parameters for the coating process with MPNs of the QCM crystal stating the amount and concentration of the phenol and iron solution added and the number of repetitions for each experiment. For the coating process the phenol and iron solution are combined with water and MOPS is added subsequently.....	13
Table 2: Concentrations of the Phenol-solutions used for the MPN dipping experiment of the QCM crystal and number how often each experiment was repeated. The QCM crystal is dipped into the solutions in succession to coat it.	13
Table 3: Summary of QCM disassembly experiments carried out. Including the mass of the MPN layer prior to disassembly, the disassembly conditions, and the type of MPN coating.	14
Table 4: Concentrations and volumes of the Phenol and Fe^{3+} solutions mixed to optimize the ratio. Additional water was added for CaAc-Fe to decrease the intensity of the complex. CaAc-Fe and pCA-Fe were mixed to achieve specific molar ratios. For LS-Fe mass ratios (mass LS:mass $\text{FeCl}_3 \cdot 6\text{H}_2\text{O}$) were used, since the molar mass of LS is unknown.*concentration of $\text{FeCl}_3 \cdot 6\text{H}_2\text{O}$	15
Table 5: Concentration of Phenol and Metal-salt used for the stepwise coating of the UV-Vis cuvettes. Water, phenol- and iron-solution were mixed to reach the concentrations stated and to coat the cuvettes.	16
Table 6: Concentration of Phenol and Metal-salt used for the examination of time on the coating of the UV-Vis cuvettes. The coating solution containing the phenol and metal were kept in the cuvette and only removed for the measurement.....	17
Table 7: Concentration of Phenol and Metal-salt used for the coating of glass slides for contact angle measurement. The glass slides were put into a glass vial and combined with water, phenol- and Fe^{3+} -solution.....	19
Table 8: Concentration of Phenol and Metal-salt used for the coating of human hair. The hair was combined with water, phenol- and Fe^{3+} -solution in a centrifuge tube and stayed in the solution for at least 10 minutes.	20
Table 9: Measurement parameters used for measuring IR-spectra	20
Table 10: Measured average mass gain after the dipping steps for different MPNs during the dipping process.....	23
Table 11: Summary of most important results of this thesis for Phenol-Iron(III) MPN experiments.○ Successful experiment/formation,△ partial successful or only successful with limitations,× not successful,- not examined. *blue color was only slightly visible.....	53

Table 12: Summary of parameters for all capsule experiments and their results. *The mass ratio of Phe: Metal-salt is given for LS, for the other components the molar ratio was used 69

Table 13: Contact angle of 3 times MPN coated glass slides. The slides were washed prior to coating and 3.1 μ l water drops were dropped on them for contact angle measurement. 70

10 Appendix

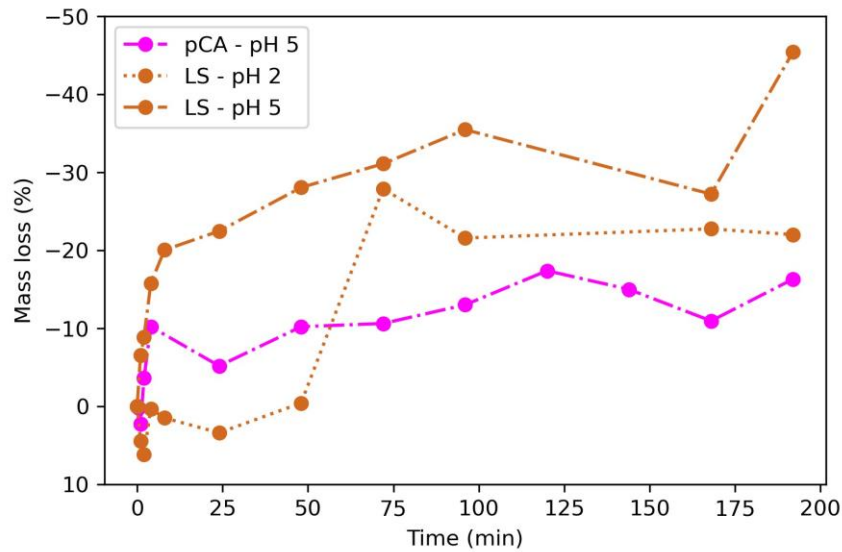


Figure 45: Results of the QCM disassembly experiment for pCA-Fe and LS-Fe coated QCM crystals. A negative mass loss indicates mass gain. The starting mass of the layer was between 729 and 1299 ng.

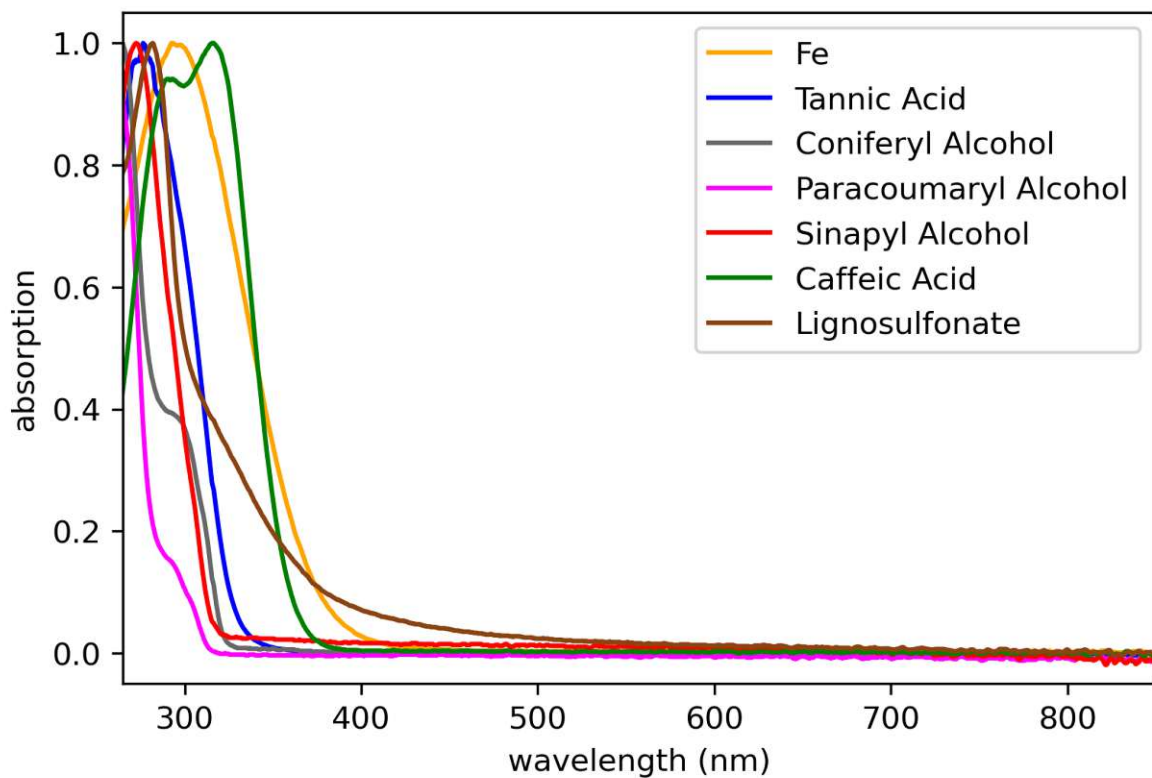


Figure 46: Spectra of iron(III)chloride and all phenols examined in the thesis in aqueous solution.

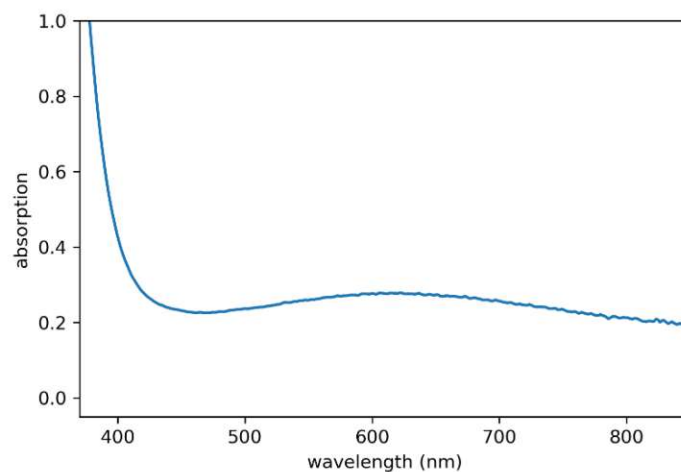


Figure 47: Spectrum of the paracoumaryl alcohol and iron solution showing the LMCT band

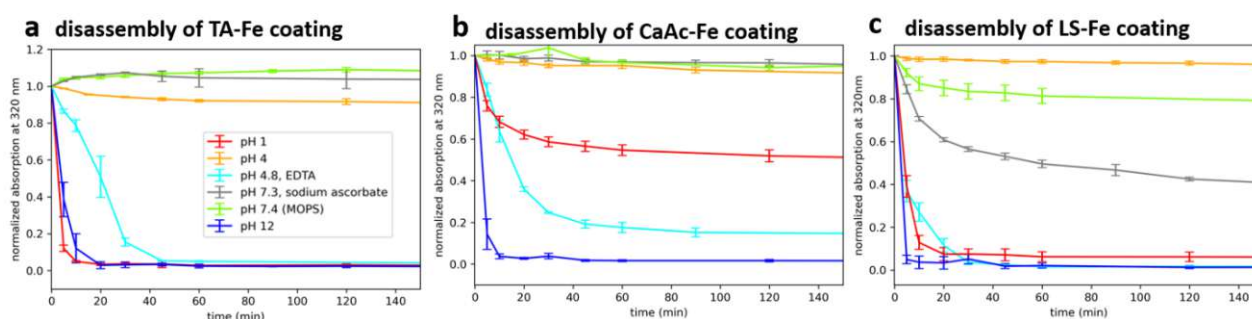


Figure 48: Disassembly of the MPN layers at different conditions, monitored by UV-Vis spectrophotometry. a) disassembly of the TA-Fe layer, b) disassembly of the CaAc-layer, c) disassembly of the LS-Fe layer

Table 12: Summary of parameters for all capsule experiments and their results. *The mass ratio of Phe: Metal-salt is given for LS, for the other components the molar ratio was used

Type of capsule	Layers	C_{Phenol} g/l	$C_{\text{FeCl}_3 \cdot 6\text{H}_2\text{O}}$ g/l	ratio Phe:Fe*	Comments	Results
TA - Fe	2	0.20	0.050	1:1.6	MOPS added	a few capsules and still PS remnants
TA - Fe	2	0.20	0.050	1:1.6	MOPS added	positive - good capsules
TA - Fe	1	0.20	0.050	1:1.6		positive - good capsules
TA - Fe	1	0.48	0.12	1:1.6		positive - good capsules
CaAc - Fe	1	1.0	1.0	3:2	no vortexing	no capsules - green precipitate
CaAc - Fe	2	2.0	2.0	3:2	no vortexing	no capsules - green precipitate
CaAc - Fe	1	1.0	3.0	1:2	no vortexing	capsules aggregate
CaAc - Fe	1	0.25	0.75	1:2		capsules aggregate
CaAc - Fe	1	0.25	0.75	1:2	2 μl 1 M NaOH added	no good results – a lot of debris
CaAc - Fe	1	0.25	0.75	1:2		microscope, SEM and TEM pictures obtained
CaAc - Fe	1	0.50	1.5	1:2		positive - good capsules

CaAc - Zr	1	0.80	0.36	4:1		no capsules - a lot of precipitate
CaAc - Zr	1	0.20	0.089	4:1		no capsules - a lot of precipitate
CaAc - Zr	2	0.20	0.36	1:1		no capsules - almost no precipitate
LS - Fe	1	4.0	2.0	2:1		very few capsules
LS - Fe	2	12	3.0	4:1		no capsules
LS - Fe	2	12	3.0	4:1		no capsules
LS - Fe	1	4.0	4.0	1:1		positive - many damaged capsules
LS - Fe	1	1.0	1.0	1:1		positive - less capsules than previous attempt
LS - Fe	1	2.0	2.0	1:1	no vortexer used	many capsules, shape a bit better
LS - Fe	1	2.0	2.0	1:1	stay in THF	SEM pictures taken, but no good capsules observed
LS - Fe	2	1.5	1.5	1:1		brittle capsules, a lot of debris
LS - Fe	1	1.0	1.0	1:1		brittle capsules, a lot of debris
pCA - Fe	2	0.01	0.050	1:2	MOPS added	No capsules, Fe precipitate
pCA - Fe	2	0.01	0.050	1:2		No capsules, Fe precipitate
pCA - Fe	1	0.01	0.050	1:2	NaCl added	no capsules
pCA - Fe	3	0.01	0.050	1:2	NaCl and EtOH added	no capsules
pCA - Fe	1	1.1	2.0	1:1		no capsules
pCA - Fe	1	1.1	2.0	1:1	10 μ l 1 M NaOH added	no capsules

Table 13: Contact angle of 3 times MPN coated glass slides. The slides were washed prior to coating and 3.1 μ l water drops were dropped on them for contact angle measurement.

	not washed		Pre-washed	
	Contact Angle (°)	Error (°)	Contact Angle (°)	Error (°)
Glass	59.6	1.8	25.8	6.7
Tannic acid - Fe	35.4	6.1	44.5	5.8
Caffeic acid - Fe	34.4	3.2	49.6	4.8
Lignosulfonate - Fe	44.9	1.6	81.2	3.1